ELSEVIER Mathematical Biosciences 151 (1998) 1–49

Mathematical Biosciences
an international journal

Mathematical models of purine metabolism in man

Raul Curto [a], Eberhard O. Voit [b], Albert Sorribas [c], Marta Cascante [a,*]

[a] *Departament de Bioquímica i Biología Molecular, Facultat de Químiques, Universitat de Barcelona, Ci Marti i Franques, 1, 08028 Barcelona, Catalunya, Spain*

[b] *Department of Biometry and Epidemiology, Medical University of South Carolina, Charleston, SC 29425-2503, USA*

[c] *Departament de Ciències Mèdiques Bàsiques, Facultat de Medecina, Universitat de Lleida, 25198 Lleida, Catalunya, Spain*

Received 27 November 1996; received in revised form 2 February 1998

Abstract

Experimental and clinical data on purine metabolism are collated and analyzed with three mathematical models. The first model is the result of an attempt to construct a traditional kinetic model based on Michaelis–Menten rate laws. This attempt is only partially successful, since kinetic information, while extensive, is not complete, and since qualitative information is difficult to incorporate into this type of model. The data gaps necessitate the complementation of the Michaelis–Menten model with other functional forms that can incorporate different types of data. The most convenient and established representations for this purpose are rate laws formulated as power-law functions, and these are used to construct a Complemented Michaelis–Menten (CMM) model. The other two models are pure power-law representations, one in the form of a Generalized Mass Action (GMA) system, and the other one in the form of an S-system. The first part of the paper contains a compendium of experimental data necessary for any model of purine metabolism. This is followed by the formulation of the three models and a comparative analysis. For physiological and moderately pathological perturbations in metabolites or enzymes, the results of the three models are very similar and consistent with clinical findings. This is an encouraging result since the three models have different structures and data requirements and are based on different mathematical assumptions.

* Corresponding author. Tel.: +34-3 402 1593; fax: +34-3 402 1219; e-mail: marta@sun.bq.ub.es.

PII: S0025-5564(98)10001-9

Significant enzyme deficiencies are not so well modeled by the S-system model. The CMM model captures the dynamics better, but judging by comparisons with clinical observations, the best model in this case is the GMA model. The model results are discussed in some detail, along with advantages and disadvantages of each modeling strategy.

Keywords: Biochemical systems theory; General mass action system; Mathematical model; Purine metabolism; S-system

Abbreviations

Abbreviation	*Metabolite*	*Variable*
PRPP	Phosphoribosylpyrophosphate	X_1
IMP	Inosine monophosphate	X_2
S-AMP	Adenylosuccinate	X_3
Ado	Adenosine	X_4
AMP	Adenosine monophosphate	
ADP	Adenosine diphosphate	
ATP	Adenosine triphosphate	
SAM	S-adenosyl-L-methionine	X_5
Ade	Adenine	X_6
XMP	Xanthosine monophosphate	X_7
GMP	Guanosine monophosphate	X_8
GDP	Guanosine diphosphate	
GTP	Guanosine triphosphate	
dAdo	Deoxyadenosine	X_9
dAMP	Deoxyadenosine monophosphate	
dADP	Deoxyadenosine diphosphate	
dATP	Deoxyadenosine triphosphate	
dGMP	Deoxyguanosine monophosphate	X_{10}
dGDP	Deoxyguanosine diphosphate	
dGTP	Deoxyguanosine triphosphate	
RNA	Ribonucleic acid	X_{11}
DNA	Deoxyribonucleic acid	X_{12}
HX	Hypoxanthine	X_{13}
Ino	Inosine	
dIno	Deoxyinosine	
Xa	Xanthine	X_{14}

Gua	Guanine	X_{15}
Guo	Guanosine	
dGuo	Deoxyguanosine	
UA	Uric acid	X_{16}
R5P	Ribose-5-phosphate	X_{17}
Pi	Phosphate	X_{18}

Abbreviation	*Full name*
GMA	Generalized Mass Action
BST	Biochemical Systems Theory
MCT	Metabolic Control Theory
CMM	Complemented Michaelis–Menten
BW	Body weight

Abbreviated flux	*Abbreviated enzyme*	*Enzyme catalyzed reaction*	*E.C.*
v_{prpps}	PRPPS	Phosphoribosylpyrophosphate synthetase	2.7.6.1.
v_{gprt}	HGPRT	Hypoxanthine-guanine phosphoribosyltransferase	2.4.2.8.
v_{hprt}	HGPRT	Hypoxanthine-guanine phosphoribosyltransferase	2.4.2.8.
v_{aprt}	APRT	Adenine phosphoribosyl-transferase	2.4.2.7.
v_{den}	ATASE	'De novo synthesis' (Amidophosphoribosyl-transferase)	2.4.2.14.
v_{pyr}		'pyrimidine synthesis'	several enzymes
v_{asuc}	ASUC	Adenylosuccinate synthetase	6.3.4.4.
v_{asli}	ASLI	Adenylosuccinate lyase	4.3.2.2.
v_{impd}	IMPD	IMP dehydrogenase	1.1.1.205.
v_{gmps}	GMPS	GMP synthetase	6.3.4.1.
v_{ampd}	AMPD	AMP deaminase	3.5.4.6.
v_{gmpr}	GMPR	GMP reductase	1.6.6.8.
v_{trans}	MT	'transmethylation pathway' (Protein O-methyltransferase)	2.1.1.24.
v_{mat}	MAT	Methionine adenosyltransferase	2.5.1.6.
v_{polyam}	SAMD	'Polyamine pathway' (S-adenosylmethionine de-carboxylase)	4.1.1.50.
v_{ade}		'Adenine oxidation' (xanthine oxidase)	1.2.1.37.

v_{inuc}	5NUC	5′-Nucleotidase	3.1.3.5.
v_{gnuc}	5NUC	5′-Nucleotidase	3.1.3.5.
v_{arna}	RNAP	RNA polymerase (from ATP)	2.7.7.6.
v_{grna}	RNAP	RNA polymerase (from GTP)	2.7.7.6.
v_{rnaa}	RNAN	RNases (to AMP)	several enzymes
v_{rnag}	RNAN	RNases (to GMP)	several enzymes
v_{dgnuc}	3NUC	5′(3′) Nucleotidase	3.1.3.31.
v_{ada}	ADA	Adenosine deaminase	3.5.4.4.
v_{dada}	ADA	Adenosine deaminase	3.5.4.4.
v_{adrnr}	DRNR	Diribonucleotide reductase	1.17.4.1.
v_{gdrnr}	DRNR	Diribonucleotide reductase	1.17.4.1.
v_{gua}	GUA	Guanine hydrolase	3.5.4.3.
v_{adna}	DNAP	DNA polymerase (from dATP)	2.7.7.7.
v_{gdna}	DNAP	DNA polymerase (from dGTP)	2.7.7.7.
v_{dnaa}	DNAN	DNases (to dAMP)	several enzymes
v_{dnag}	DNAN	DNases (to dGMP)	several enzymes
v_{hx}		‘Hypoxanthine excretion’	Non-enzymatic step
v_{hxd}	XD	Xanthine oxidase or xanthine dehydrogenase	1.2.1.37.
v_{xd}	XD	Xanthine oxidase or xanthine dehydrogenase	1.2.1.37.
v_{x}		‘Xanthine excretion’	Non-enzymatic step
v_{ua}		‘Uric acid excretion’	Non-enzymatic step

1. Introduction

Purine metabolism constitutes a key pathway for every organism since it is at the heart of DNA and RNA synthesis and degradation and involves the production of ubiquitous metabolites like ATP. It is also clinically important because of numerous diseases, ranging from gout to mental retardation, that are associated with well-characterized enzyme defects of this pathway.

The literature contains an enormous amount of data about purine metabolism in different species, tissues, and under different metabolic and physiological conditions. Even so, there are very definite gaps in our knowledge about the pathway, and the complexity of the regulatory mechanisms and the large number of branches in this pathway make it very difficult to understand and predict its behavior intuitively.

A promising approach to understanding purine metabolism is the construction and analysis of a mathematical model that is able to deal with large

numbers of metabolites and complex interactions. Such an approach is feasible since purine metabolism constitutes an almost closed pathway in which only a few metabolites are products of, or substrates for, other pathways. In our model definition, the metabolic system consists of sixteen dependent variables, two independent variables and thirty-seven steps; it is depicted in Fig. 1.

Several approaches to modeling purine metabolism were developed in recent years. Franco and Canela [1] designed one of the first kinetic models of purine metabolism based on data from different species and tissues, with the aim of demonstrating the usefulness of computer simulations of complex metabolic networks. Heinmets [2] modeled nucleic acid synthesis from nucleotides and deoxynucleotides, but the model parameters were not directly obtained from experimental data. More recently, Bartel and Holzhütter [3] constructed a model based on rat liver as the reference system.

The goal of the present paper is to develop an integrated model that is based on available data and that may aid our understanding of the complex dynamics of purine metabolism. Our reference system is the whole human body. This is a daring task, but it seems that in the long run it will be the only way to address the large and diverse amount of experimental and clinical data on normal and deficient purine metabolism and potential treatments. Furthermore, it would appear to be restrictive to focus on a single cell type or tissue, since the pathways of purine metabolism are distributed among several tissues at different locations throughout the body [4,5].

In order not to become overwhelmed with complexity, the prototype models presented here do not account for the physiological compartmentalization of purine metabolism throughout the body. This is a potentially significant simplification that should be addressed in the future. However, at this point, a non-compartmental model seems to be a reasonable starting point for understanding some aspects the complex dynamics of purine metabolism. The future inclusion of compartments in an overall model must be expected to be a challenge, since some pathways within purine metabolism differ among tissues and even at the cellular level [6]. Since there are no absolute guidelines for the choice of a particular model, we develop three alternative models and compare them with each other and with clinical observations. This comparison may help future researchers with model selection in similar situations.

The first and most significant step for this comparative analysis is the assessment of experimental data from the literature. For this step, we collected published information on metabolite concentrations, flux values, and enzyme kinetics from both biochemical and clinical studies. The evaluation of this information is useful not only in the context of the present paper, but it is a necessary prerequisite for any modeling approach to understanding purine metabolism. Because of the importance of this step, we discuss data collection and parameter estimation in some detail.

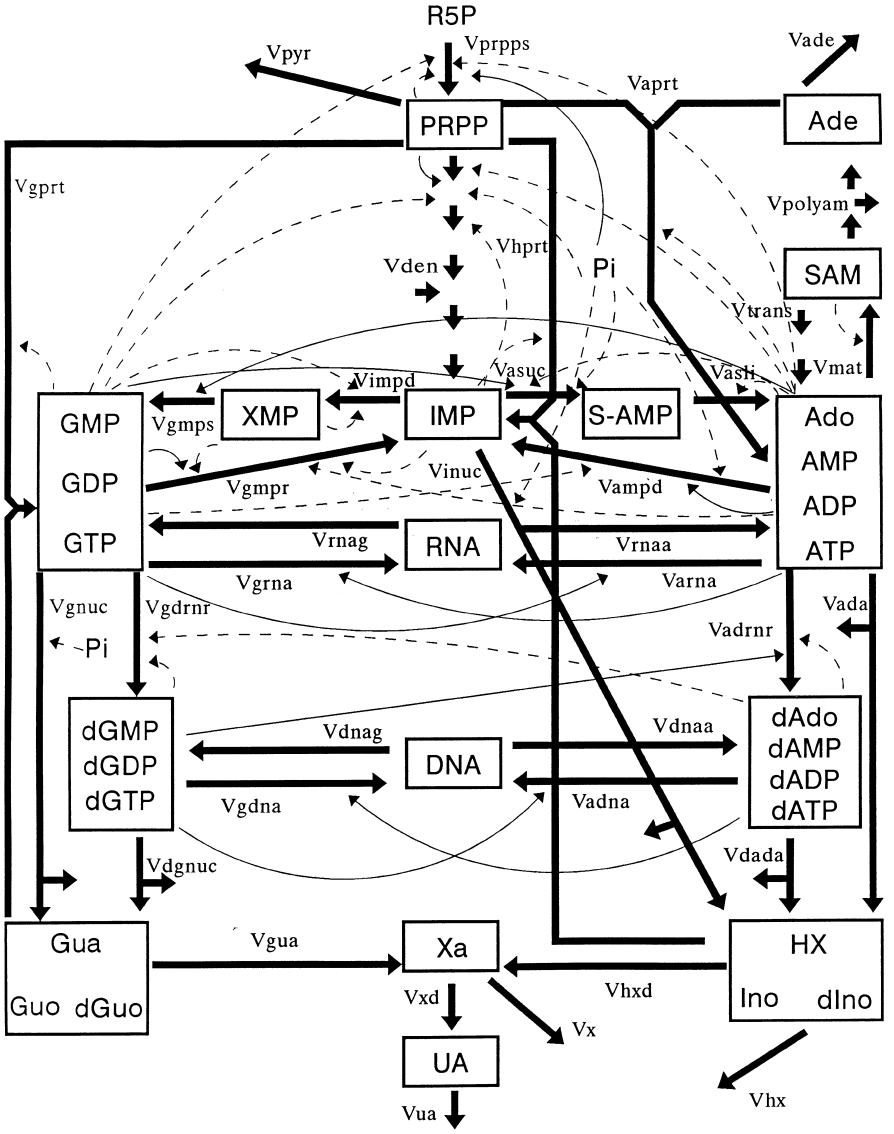

Fig. 1. Metabolic diagram of purine metabolism in man. Dependent variables are shown in boxes, independent variables (R5P and Pi) without boxes. Fluxes are represented by straight, heavy arrows and identified with abbreviated names. Regulatory signals are represented by curved, light arrows; inhibitions are indicated by dashed lines and activations by solid lines (for names of metabolites and fluxes, see Section *Abbreviations*).

The literature contains considerable information about the key processes of the pathway, and this information is often presented in the form of parameters such as K_M, V_{MAX}, and K_I. This information can be directly translated into traditional Michaelis–Menten or Hill rate laws. However, the published information is not complete, especially, if one restricts the search to human cells. In some cases, the lack of information can be alleviated with direct or indirect data, obtained in vivo or in vitro, that show how one variable affects the rate of a particular step. While this information is insufficient for translating these observations into corresponding Michaelis–Menten equations, it can be used to formulate and parameterize power-function rate laws proposed in Biochemical Systems Theory (BST) [7–13].

The first model we analyze is a 'Complemented Michaelis–Menten' (CMM) model in which as many steps of the pathway as currently possible (15 out of the 37) are expressed as traditional Michaelis–Menten rate laws, 10 are expressed as power-law rate laws, and 12 are mixed.

The other two models are formulated as canonical models within the framework of BST. The first of these is a Generalized Mass Action (GMA) model in which each individual step is represented as power-function rate law. These representations are readily obtained directly from data or from the previously defined CMM model, with methods that are well documented in the literature [10,14].

The second power-law model is given in the form of an S-system. In this form, influxes and outfluxes at branchpoints are aggregated into one power-law term each. This form is simpler in structure and allows analytic evaluations of the steady-state that are not possible in other types of models. It was also shown in a theoretical setting [14] that S-systems capture the dynamics of pure Michaelis–Menten models better than GMA systems, if the involved metabolites vary within physiological ranges. If the metabolites deviate greatly from their nominal values, either one of the power-law models may be more accurate [14]. Our results here confirm that this is true for purine metabolism. For small perturbations, the responses of the S-system model are slightly closer to CMM than GMA, but for very large perturbations, as they occur in severe enzyme deficiencies, the GMA model agrees significantly better with clinical observations than the S-system model. Reasons for this result, along with advantages and disadvantages of the three models, are discussed in the final section of the paper.

2. Mathematical representation and data requirements

A standard concept for describing the dynamics of complex systems is based on mass balance equations of the type

$$\dot{X}_i = \sum_{j=1}^{r} c_{ij} v_j, \tag{1}$$

where r is the number of processes in the system, and the processes v_j are functions of some or all of the metabolites X_i. The parameters c_{ij} are the stoichiometric coefficients of the reaction v_j in the equation of metabolite X_i. These coefficients take values: greater than 0, if v_j synthesizes X_i; equal to 0, if v_j has no effect on X_i; and lower than 0, if v_j degrades X_i.

In traditional enzyme kinetics, the functions v_j represent enzyme catalyzed processes, each of which is formulated as a rational function that relates the reaction rate with the concentrations of substrates and modulators. The simplest example is the Michaelis–Menten equation

$$v_i = \frac{V_{\mathrm{MAX}} X_j}{K_M + X_j}, \tag{2}$$

which has been the paradigm rate law for almost a century [15]. It has proven very useful in itself and has also been used as the basis for more complicated rate laws involving activators, inhibitors, allosteric substrates, and other modulating influences.

For reactions that include several substrates, products, or modulators, the traditional rate laws become unwieldy, and this has prompted the search for alternative representations. Valid, yet mathematically convenient substitutes for the traditional rate laws are particularly needed if the objective of the investigation is the analysis of realistically sized, integrated metabolic pathways and their dynamic behavior. Addressing this need, BST [9,13] was developed as a mathematically rigorous modeling approach that can make use of a wide variety of data and other types of more qualitative information. In BST, each rate is represented by a product of power-law functions. This strategy has empirically proven successful and is mathematically justified, since it derives from linear approximation of the rate in logarithmic space. The power-law representation is equivalent with the actual rate law at any chosen operating point, but the two typically differ when the system moves away from this point. Experience suggests that the rate laws in BST are sufficiently accurate if the metabolites in the pathway remain within their physiological ranges.

For the GMA model, the rate laws are formulated as

$$v_i = \alpha_i \prod_{j=1}^{n+m} X_j^{f_{ij}}. \tag{3}$$

In this representation, n is the number of dependent variables and m the number of independent variables (in the case of purine metabolism, $n = 16$ and $m = 2$), and α_i is the rate constant of the reaction. The kinetic orders f_{ij} are the normalized partial derivatives of fluxes with respect to the involved metabolite or modulator concentrations; they are equivalent to elasticity coefficients in Metabolic Control Theory (MCT) [10,16,17]

$$\left(\frac{\partial v_i}{\partial X_j}\right)_0 \frac{X_{j_0}}{V_{i_0}} = f_{ij}. \tag{4}$$

This interpretation of kinetic orders provides a straightforward procedure for translating traditional rate laws into GMA rate laws (see Appendix A for illustrations).

An alternative to the GMA power-law model is an S-system model. The rationale again is representation in logarithmic space of the actual and unknown rate law, but instead of approximating each step separately, all fluxes of synthesis of a given dependent variable are aggregated in only one power-law term and all fluxes of degradation are aggregated in one power-law term. As a result, the typical S-system equation contains two terms and reads

$$\mathring{X}_i = \alpha_i \prod_{j=1}^{n+m} X_j^{g_{ij}} - \beta_i \prod_{j=1}^{n+m} X_j^{h_{ij}}. \tag{5}$$

As before, n is the number of dependent variables (16) and m the number of independent variables (2); α_i and β_i are the rate constants for the synthesis and degradation processes of the reaction; and g_{ij} and h_{ij} are the kinetic orders of the metabolite or modulator j in the synthesis or degradation of metabolite i, respectively.

The transition from the GMA model to the S-system model is straightforward, since the S-system parameters are computed by partial differentiation from the collections of GMA terms that describe all influxes or all outfluxes for each dependent variable

$$g_{ij} \text{ or } h_{ij} = \sum_{r=1}^{l} f_{i_r,j} \left(\frac{v_{i_r}}{\sum_{s=1}^{l} v_{i_s}} \right)_0. \tag{6}$$

Here, v_{i_r} and v_{i_s} represent the individual steps for the synthesis or degradation of the metabolite X_i, l is the number of individual steps that constitute the aggregated synthesis or degradation of the metabolite X_i, and the parameters f_{i_r} are the kinetic orders in GMA of the variable X_j with respect to the rth step of synthesis or degradation of metabolite X_i.

The maximal velocities V_{VIVO} in the CMM rate laws and the rate constants in the power-law models are defined in such a way that the steady-state concentrations of metabolites give the desired steady-state values for fluxes.

3. Estimation of parameters from experimental data

It is quite evident that any in vivo parameter estimates are subject to great uncertainty. This uncertainty is composed of two types, sometimes referred to as *natural variability* or *Type A* and *true uncertainty* or *Type B* [18]. The natural variability accounts for the situation that the parameter in question is uniquely given but unknown, whereas the true uncertainty accounts for the situation that the parameter indeed is distributed. Clearly, both types of uncertainty are relevant in purine metabolism, and this must be remembered when results are presented and interpreted.

3.1. Steady-state operating point

The first step in the estimation of parameter values is the choice of an operating point, which is characterized by a set of concentrations and fluxes that represent a physiological steady state in humans. Of course, this steady state varies from person to person and also is affected by diet and the degree of physical activity, and we chose a hypothetical average situation that appeared to be realistic. Sensitivity tests [19] have shown that this steady state in fact is rather robust and that moderate changes in kinetic parameters of the model do not affect the fluxes or concentrations much (see also below). The steady-state concentrations are presented in Table 1, along with clinical measurements in different tissues and with references.

3.2. Fluxes and flux constraints

The estimation of fluxes is the most difficult step in constructing kinetic models, because there are few direct measurements of fluxes in the intact human body. However, using indirect information about the amount of a chemical compound that is metabolized during a given period of time and an average body weight (BW) of 70 kg, we can deduce several of the required fluxes. We selected μmol min^{-1} BW^{-1} as units of flux, being those units the number of μmols transformed per minute in the whole human body, assuming an average weight of 70 kg.

The model contains 37 fluxes (cf. Fig. 1). Given steady-state values for the 16 dependent variables, 16 of the fluxes can be formulated as linear combinations of the remaining 21. The resulting steady-state flux equations are

X_1: $v_{prpps} = v_{gprt} + v_{hprt} + v_{aprt} + v_{den} + v_{pyr}$,
X_2: $v_{den} + v_{gmpr} + v_{ampd} + v_{hprt} = v_{impd} + v_{asuc} + v_{inuc}$,
X_3: $v_{asuc} = v_{asli}$,
X_4: $v_{aprt} + v_{asli} + v_{trans} + v_{rnaa} = v_{mat} + v_{ampd} + v_{arna} + v_{adrnr} + v_{ada}$,
X_5: $v_{mat} = v_{trans} + v_{polyam}$,
X_6: $v_{polyam} = v_{aprt} + v_{ade}$,
X_7: $v_{impd} = v_{gmps}$,
X_8: $v_{gmps} + v_{rnag} + v_{gprt} = v_{gmpr} + v_{grna} + v_{gdrnr} + v_{gnuc}$,
X_9: $v_{adrnr} + v_{dnaa} = v_{adna} + v_{dada}$,
X_{10}: $v_{gdrnr} + v_{dnag} = v_{gdna} + v_{dgnuc}$,
X_{11}: $v_{arna} + v_{grna} = v_{rnag} + v_{rnaa}$,
X_{12}: $v_{adna} + v_{gdna} = v_{dnag} + v_{dnaa}$,
X_{13}: $v_{ada} + v_{dada} + v_{inuc} = v_{hprt} + v_{hxd} + v_{hx}$,
X_{14}: $v_{hxd} + v_{gua} = v_{xd} + v_{x}$,
X_{15}: $v_{dgnuc} + v_{gnuc} = v_{gprt} + v_{gua}$,
X_{16}: $v_{xd} = v_{ua}$.

Table 1
Estimation of metabolite concentrations (units for concentrations are in μM)

Variables	Conc.	Metabolite	Conc.	Tissue	Conc.	Refs.	Comments
X_1	5	PRPP	5	Human cells	5	[55]	
				Human erythrocytes	2–7	[55]	
				Human cells	<10	[56]	
X_2	100	IMP	100	Human liver	120–300	[57]	1
				Human kidney	50–110		
				Human erythrocytes	5–85		
				Human brain	17	[58]	
X_3	0.2	S-AMP	0.2	Rat muscle	<0.2	[59]	2
X_4	2500	AMP	200	Rat muscle	93	[59]	
				Rat liver	270	[60]	
				Rat erythrocytes	37		
				Erlich cells	500–700	[61]	
				Glioblastoma	241	[58]	
				Human brain	242		
		ADP	400	Rat muscle	624	[59]	
				Rat liver	530	[60]	
				Rat erythrocytes	174		
				Glioblastoma	527	[58]	
				Human brain	788		
		ATP	1900	Rat muscle	5000	[59]	
				Rat liver	1512	[60]	
				Rat erythrocytes	1702		
				Glioblastoma	1105	[58]	
				Human brain	2100		
		Ado	0.5	General tissues	0.5	[30]	
X_5	4	SAM	4	Human erythrocytes	3.5	[62,63]	
X_6	1	Ade	1	Erlich cells	1.4	[64]	
				Rat liver	0.9	[60]	
				Rat muscle	1.3		
				Rat erythrocytes	1.6		
				Rat plasma	3.2		
				Human brain	4.5	[58]	
				Human plasma	0.07	[65]	
X_7	25	XMP	25	Not infected cells	= [GMP]	[66]	
X_8	400	GMP	25	Glioblastomas	22	[58]	
				Human brain	26		
		GDP	75	Human erythrocytes	33	[67]	
				Erlich cells	220	[64]	
				Glioblastoma	74	[58]	
				Human brain	169		
		GTP	300	Human erythrocytes	205	[67]	
				Erlich cells	350	[64]	

Table 1 *(continued)*

Variables	Conc.	Metabolite	Conc.	Tissue	Conc.	Refs.	Comments
				Glioblastoma	225	[58]	
				Human brain	300		
X_9	6	dAdo	0.1	Human brain	<0.1	[58]	
		dAMP	0.5	General tissues		[31,68]	3
		dADP	1.4				
		dATP	4				
X_{10}	3	dGMP	0.1	General tissues		[31,68]	3
		dGDP	0.5				
		dGTP	2.4				
X_{11}	28600	RNA	28600	Mammalian organisms	6 [DNA]	[69]	
				D discoideum	30000	[70]	
X_{12}	5160	DNA	5160	Human body	5160	[71]	4
X_{13}	10	HX	6.9	Rat interstitial fluid	7.2	[30]	
				Human plasma	1.7	[72]	
				Human bone marrow	7.1	[73]	
				Human plasma	2.4		
				Glioblastoma	30	[58]	
				Human brain	32		
		Ino	3	Rat liver	4.7	[60]	
				Rat muscle	2.4		
				Rat erythrocytes	2.6		
				Rat plasma	2.1		
				Human plasma	0.9	[72]	
				Glioblastoma	30	[58]	
				Human brain	27		
		dIno	0.1	Human brain	<0.1	[58]	
X_{14}	5	Xa	5	Human plasma	0.9	[74]	
				Human CSF	2		
				Xanthinuric patient	8	[21]	
				Glioblastoma	32	[58]	
				Human brain	34		
X_{15}	5	Gua	0.5	Glioblastoma	0.6	[58]	
				Human brain	0.4		
		Guo	4.4	Rat liver	6.9	[60]	
				Rat muscle	4.5		
				Rat erythrocytes	1.7		
				Rat plasma	0.8		
				Glioblastoma	6.2	[58]	
				Human brain	5.3		
		dGuo	0.1	Human brain	<0.1	[58]	
				PNP deficient patient	1	[67]	

Table 1 *(continued)*

Variables	Conc.	Metabolite	Conc.	Tissue	Conc.	Refs.	Comments
X_{16}	100	UA	100	Human body	100	[20]	
X_{17}	18	R5P	18	Mouse liver	18	[69]	
X_{18}	1400	Pi	1400	Eukaryotic cells	400–6000	[75]	
				Rat cardiomyocytes	1400	[76]	
				Human erythrocytes	1000	[77]	

Comments: (1) The IMP concentration can vary considerably with the metabolic and physiological conditions. Some of these variations are due to the differences in metabolism during rest (when IMP concentration is lower) and during exercise (when IMP is higher). (2) No concentrations were found for this metabolite in human tissues. (3) The concentrations of deoxynucleotides are very difficult to estimate. When cells are in stationary phase, the deoxynucleotides cannot be detected; they can only be measured when cells are dividing. In the latter case, the concentrations are of the order of 20 μM [68]. Furthermore, one can assume that deoxynucleotides are less than 1% of the corresponding nucleotides [31]. (4) The human body contains about 75×10^{12} cells, and each cell contains 2.9×10^9 base pairs. Using these parameters, we arrive at a concentration of 5160 μM for purine nucleotides bound in DNA.

In addition to these steady-state constraints, it is known that the ratio of adenine and guanine in nucleic acids is approximately $\frac{3}{2}$. This fact allows us to formulate four more constraints between the fluxes in steady state:

$v_{\text{arna}} = \frac{3}{2} v_{\text{grna}}$,
$v_{\text{rnaa}} = \frac{3}{2} v_{\text{rnag}}$,
$v_{\text{adna}} = \frac{3}{2} v_{\text{gdna}}$,
$v_{\text{dnaa}} = \frac{3}{2} v_{\text{dnag}}$.

While very helpful, these constraints are not sufficient for a complete kinetic characterization. Seventeen more flux estimates or constraints between fluxes are needed, and these have been extracted from experimental data. The results are presented in Table 2 and explained in the following. The fluxes with non-explicitated units have the implicit units of μmol min^{-1} BW^{-1}.

(1) The first equation reflects in vivo measurements of the amount of UA excreted in urine. Normal subjects excrete 418–426 mg per day of UA in urine [20]. However, only 75% of the total UA excretion appear in urine, while the remaining 25% are excreted by the gut as allantoine or as other catabolites [20]. The flux thus has to be increased by $\frac{4}{3}$, which yields the final value of 2.27.

(2) Strictly speaking, data obtained from xanthinuric patients (usually individuals with XD deficiency) are not valid for our model, because they do not derive from healthy subjects. Nevertheless, they provide the only quantitative information on this flux. The excretion of oxypurines in xanthinuric subjects is about 300 mg per day [21], which is approximately the same as UA excretion in healthy subjects. The xanthinuric subjects in Bradford's [21] study had no other relevant disorders of purine metabolism, with the exception of large

Table 2
Experimentally based flux equations

Number	Equation	References
1	$v_{ua} \simeq 2.27$ μmol min^{-1} BW^{-1}	[20]
2	$v_{hxd} + v_{hprt} \simeq 4.9$ μmol min^{-1} BW^{-1}	[21]
3	$v_{hprt} \simeq 3 \times v_{hxd}$	[20,22]
4	$v_{hprt} \simeq v_{gprt}$	[23,24]
5	$v_{gdrnr} + v_{gnuc} \simeq 9 \times v_{gmpr}$	[24,25]
6	$v_{asuc} \simeq 5 \times v_{impd}$	[26,27]
7	$v_{aprt} \simeq 1$ μmol min^{-1} BW^{-1}	[28]
8	$\frac{v_{ada}}{v_{dada}} \simeq \frac{[Ado]}{[dAdo]} \simeq 10$	[30]
9	$\frac{v_{gnuc}}{v_{dgnuc}} \simeq \frac{[GMP]}{[dGMP]} \simeq 250$	The same assumption as in Eq. (8)
10	$v_{trans} \simeq 14$ μmol min^{-1} BW^{-1}	[31]
11	$v_{pyr} \simeq 10$ μmol min^{-1} BW^{-1}	Assuming that purine synthesis is of the same order of pyrimidine synthesis
12	$v_{ade} \simeq 0.01$ μmol min^{-1} BW^{-1}	[78]
13	$v_{hx} \simeq 0.05$ μmol min^{-1} BW^{-1}	[33]
14	$v_{x} \simeq 0.03$ μmol min^{-1} BW^{-1}	[33]
15	$v_{ampd} \simeq 3 \times v_{ada}$	[34]
16	$v_{adna} + v_{gdna} = 17$ μmol min^{-1} BW^{-1}	[71]
17	$v_{arna} + v_{grna} = 3300$ μmol min^{-1} BW^{-1}	[35]

excretion of Xa and HX instead of UA, which in these patients is negligible. It thus appears reasonable to assume that purine metabolism in these subject is similar to that in healthy subjects, except that HX, which in healthy subjects is transformed into Xa (v_{hxd}), and Xa, which in healthy subjects is transformed into UA (v_{xd}), are excreted in larger amounts (v_{hx} and v_x). Given that the steady-state values of other fluxes are unaffected by xanthinurea, the turnover of HX in xanthinuric patients seems to provide at least a crude estimate. The HX turnover in these patient is 4.9, and this implies $v_{hprt} + v_{hxd} = 4.9$.

Based on similar arguments, one can use information about Xa turnover, which in xanthinuric subjects is about 1.26. Because the only reaction that synthesizes Xa in these patients is v_{gua}, one concludes that $v_{gua} = 1.26$. One might assume that healthy subjects had the same value of v_{gua}, but since this is not clear, we do not use this information as a constraint. Nonetheless, this estimation is in accord with the third equation in Table 2.

(3) It is generally known that most of HX is recycled by v_{hprt}, which implies that v_{hprt} is greater than v_{hxd}. Averaging available data [20,22], one can assume that v_{hprt} degrades about 75% of HX, so that $v_{hprt} = 3\ v_{hxd}$. This relationship, combined with information about the turnover of HX discussed in (2) (4.9), suggests roughly $v_{hxd} = 1.2$ and $v_{hprt} = 3.7$. Furthermore, if $v_{hxd} = 1.2$ and $v_{xd} = 2.27$ at steady-state, then $v_{gua} = 1.07$, which is close to the value obtained for xanthinuric subjects (1.26).

(4) Measurements of the activity of v_{aprt}, v_{hprt} and v_{gprt} reported in the literature suggest that the activities of hprt and gprt are similar and that the activity of aprt is less than the other two [23,24].

(5) Between 90% and 100% of guanine nucleotides are degraded to Xa [24,25]. Even though this information is not as quantitative as we would like, it roughly suggests the constraint $v_{gdrnr} + v_{gnuc} = 9\ v_{gmpr}$.

(6) The branchpoint of IMP is most important in the regulation of purine metabolism. It has been reported that the ratio v_{asuc}/v_{impd} is close to 5 in human tissues in stationary phase, while it is close to 1 during cell proliferation [26,27]. We selected a value of 5 for our system.

(7) The flux v_{aprt} was studied in an APRT deficient patient [28]. Since this subject presented with no other relevant disorders of purine metabolism (see below), one can assume that this patient synthesized the same amount of Ade as healthy subjects, but excreted it as 2,8-dihydroxyadenine instead of recycling it with v_{aprt}. If this is the case, the excretion of adenine metabolites in this patient should be equivalent to the flux of v_{aprt} in healthy subjects. Adjusted for BW, v_{aprt} thus has a value of approximately 1. Other experimental data [29] yield similar results.

(8) No direct information is available about the kinetic properties of reactions catalyzed by ADA. However, according to Geiger and Nagy [23], ADA exhibits the same activity with Ado as with dAdo. A reasonable assumption is therefore, that the proportionality between v_{ada} and Ado is probably of the same order of magnitude as the proportionality between v_{dada} and dAdo. This assumption leads to the statement in Table 2; its uncertainty is reflected by the symbol $\approx$.

(9) No hard experimental data are available to estimate what fractions of the guanine nucleotide pool are degraded by v_{gnuc} and v_{gdrnr}, respectively. One may suppose that the proportionality between these fluxes and the corresponding concentrations of the guanine nucleotides and deoxynucleotides are probably of the same order of magnitude. This assumption leads to the statement in Table 2; its uncertainty is reflected by the symbol $\approx$.

(10) Human S-adenosyl-L-homocysteine hydrolase, which is the last enzyme in the transmethylation pathway, generates between 14 and 23 mmols of Ado in 12 h [31]. This corresponds to an average flux of about 14.

(11) The flux of v_{pyr} is difficult to estimate. One may assume that the synthesis of pyrimidines is approximately equal to the synthesis of purines. A reasonable value seems to be 10.

(12) v_{ade} is less than 0.07 [29], and this flux is 0.01 or less [24,32]. We set the value as 0.01.

(13) and (14) v_{hx} and v_x for humans in vivo are about 0.05 and 0.03, respectively [33].

(15) [34] related the fluxes of v_{ampd} and v_{ada} in different tissues and suggested a ratio of about 3.

(16) If one assumes an average human cell turnover of 15 days and takes into account that DNA must be resynthesized during every cell cycle, one obtains a DNA turnover rate of 17.

(17) mRNA constitutes a mere 3% of the total RNA pool, but the turnover flux of the mRNA pool is about 30% of the turnover flux of the total RNA pool. Furthermore, the half life for mRNA in eukaryotic organisms is about 30 min [35]. These data yield an RNA turnover rate of 3300. Sander et al. [36] estimated this turnover value as 0.06 assuming one mole of RNA as the entire chain of nucleotides, whereas in our model, one mole refers to a single RNA nucleotide. For comparison, the turnover rate in Sander's analysis must therefore be multiplied with the average length of an RNA chain. If one assume that the average length of an RNA chain is about 50 000, the two estimations are very close.

With these estimates and constraints, the system of equations has a unique solution for the flux values at steady state; this solution is presented in Table 3. While these values have been calculated for our specific modeling purposes, they are interesting in themselves because they provide some insight in the distribution of fluxes in human purine metabolism.

3.3. Estimation methods

For the CMM model, we collected as many parameters as possible from experimental data in humans. Only less than half of the fluxes could be evaluated in this fashion, and we were forced to complement them with other types of rate laws. For this purpose, we estimated kinetic orders of power-law representations instead of the traditional constants K_M, K_i or K_A.

Some of the variables in our model represent pools, rather than individual metabolites. An example is the pool X_4, which includes ATP, ADP, AMP, and Ado. This needs to be considered when only one or two of the constituents

Table 3
Steady-state flux rates in man

$v_{ada} = 2.1$	$v_{ade} = 0.01$	$v_{adna} = 10$	$v_{adrnr} = 0.2$
$v_{ampd} = 5.69$	$v_{aprt} = 1$	$v_{arna} = 1980$	$v_{asuc} = 8$
$v_{asli} = 8$	$v_{dada} = 0.2$	$v_{den} = 2.39$	$v_{dgnuc} = 0.1$
$v_{dnaa} = 10$	$v_{dnag} = 6.8$	$v_{gdna} = 6.8$	$v_{gdrnr} = 0.1$
$v_{gmpr} = 0.5$	$v_{gmps} = 1.6$	$v_{gnuc} = 4.7$	$v_{gprt} = 3.7$
$v_{grna} = 1320$	$v_{gua} = 1.1$	$v_{hprt} = 3.7$	$v_{hx} = 0.05$
$v_{hxd} = 1.23$	$v_{impd} = 1.6$	$v_{inuc} = 2.68$	$v_{mat} = 15$
$v_{polyam} = 1.01$	$v_{prpps} = 20.79$	$v_{pyr} = 10$	$v_{rnaa} = 1980$
$v_{rnag} = 1320$	$v_{trans} = 13.99$	$v_{ua} = 2.3$	$v_{x} = 0.03$
$v_{xd} = 2.3$			

Variables are listed in alphabetical order. Units are μmol min^{-1} BW^{-1}.

of such pools affect a rate law. For instance, we cannot directly include ATP as a variable in a kinetic rate law, because ATP is not a dependent variable in the model. Instead, we use X_4 and correct the disparity between ATP and X_4 by multiplying X_4 in the rate law with the factor [ATP]/X_4 at the operating point. The kinetic rate law of each reaction and its associated parameter values are presented in next section.

Parameter values for the GMA model were obtained from kinetic data as shown in Eq. (4). In most cases, the kinetic orders were coded as '*f*' followed by the abbreviated name of the reaction and by the number (or abbreviated name) of the variable that affects the rate of the reaction.

The only exceptions are the kinetic orders for the synthesis and degradation of nucleic acids. These are constrained by the fact that the ratio of Ade/Gua in nucleic acids is essentially constant. To ensure that the kinetic parameters of v_{arna} and v_{grna} are the same, we coded them as $f_{\mathrm{rnap(i)}}$ (as an acronym for the enzyme RNA polymerase). Similarly, $f_{\mathrm{rnan(i)}}$ stands for the kinetic orders of v_{rnag} and v_{rnaa} (as an acronym for the enzyme RNA nucleotidase), $f_{\mathrm{dnap(i)}}$ for the kinetic orders of v_{adna} and v_{gdna} (for DNA polymerase), and $f_{\mathrm{dnan(i)}}$ for kinetic orders of v_{dnaa} and v_{dnag} (for DNA nucleotidase). This deviation in nomenclature signifies that the incorporation of guanine nucleotides to nucleic acids is proportional to the incorporation of adenine.

To estimate the GMA parameters in cases where the substrate or modifier of the reaction is an aggregated pool, we took into account that the aggregated pool concentration is the sum of the concentrations of the individual components and that the equilibrium between them is achieved very rapidly. For instance, suppose that the aggregated pool of X_j is composed of three chemical substances, X_a, X_b, and X_c:

$$X_j = X_a + X_b + X_c,$$

$$X_a \rightleftharpoons X_b \rightleftharpoons X_c.$$

Introducing the equilibrium constants $K_1 = X_{\mathrm{b}}/X_a$, $K_2 = X_c/X_b$, we can formulate the rapid equilibrium between the metabolites as

$$X_j = X_a + K_1X_a + K_2K_1X_a = X_a(1 + K_1 + K_1K_2) = K_1'X_a,$$

$$X_j = X_b + X_b/K_1 + K_2X_b = X_b(1 + 1/K_1 + K_2) = K_2'X_b,$$

$$X_j = X_c + X_c/K_2 + X_c/(K_2K_1) = X_c(1 + 1/K_2 + 1/(K_1K_2) = K_3'X_c.$$

According to Eq. (4), the parameters of interest are defined as

$$f_{ij} = \left(\frac{\partial v_i}{\partial X_j}\right)_0 \frac{X_{j_0}}{v_{i_0}}, \qquad f_{ia} = \left(\frac{\partial v_i}{\partial X_a}\right)_0 \frac{X_{a_0}}{v_{i_0}}.$$

$$f_{ib} = \left(\frac{\partial v_i}{\partial X_b}\right)_0 \frac{X_{b_0}}{v_{i_0}}, \qquad f_{ic} = \left(\frac{\partial v_i}{\partial X_c}\right)_0 \frac{X_{c_0}}{v_{i_0}}.$$

Application of the chain rule of differentiation leads to

$$f_{ij} = \left(\frac{\partial v_i}{\partial X_j}\right)_0 \frac{X_{j_0}}{v_{i_0}} = \frac{X_{j_0}}{v_{i_0}}\left[\left(\frac{\partial v_i}{\partial X_a}\right)_0\left(\frac{\partial X_a}{\partial X_j}\right)_0 + \left(\frac{\partial v_i}{\partial X_b}\right)_0\left(\frac{\partial X_b}{\partial X_j}\right)_0 + \left(\frac{\partial v_i}{\partial X_c}\right)_0\left(\frac{\partial X_c}{\partial X_j}\right)_0\right]$$

$$= \left(\frac{\partial v_i}{\partial X_a}\right)\frac{1}{K_1}\frac{K_1 X_a}{v_i} + \left(\frac{\partial v_i}{\partial X_b}\right)\frac{1}{K_2}\frac{K_2 X_b}{v_i} + \left(\frac{\partial v_i}{\partial X_c}\right)\frac{1}{K_3}\frac{K_3 X_c}{v_i}$$

and this yields, upon rearrangement of terms,

$$f_{ij} = f_{ia} + f_{ib} + f_{ic}.$$

This mathematical derivation shows that a kinetic order with respect to an aggregated pool is equal to the sum of the kinetic orders with respect to the individual components of the pool.

Some steps within purine metabolism (e.g., v_{den}, v_{polyam}, and v_{trans}) do not consist of only one reaction, but of linear pathways, and it turned out to be impossible to find kinetic rate laws for the entire sets of reactions. Theoretical arguments suggest estimating the parameters of these fluxes from the first enzyme of the pathway, as is discussed below.

First, one can argue that the kinetic orders of a flux representing a linear pathway are, by definition, the logarithmic flux gains [13] of this linear pathway. For instance, if one would construct a model of the 10 reactions that comprise v_{den}, one could calculate the logarithmic flux gains of this pathway and subsequently use them as kinetic orders in the overall model of purine metabolism.

Secondly, one can justify the use of kinetic orders associated with the first enzyme by evoking a fundamental equation of BST that relates flux gains and kinetic orders: $[L(v_i, X_k)] = [G_i] + [G_d][L(X_i, X_k)]$ [37,38]. In a linear pathway, all rows in the matrix $[L(v_i, X_k)]$ are identical because all fluxes have the same value in steady state. Thus, one needs to calculate only one row of this matrix to know all logarithmic flux gains of the system. Consider one step in the linear pathway which is not modified by any dependent variable of the pathway, and for which, consequently, all kinetic orders of the matrix G_d are zeros. The corresponding row of the matrix $[G_d][L(X_i, X_k)]$ is a row of zeros, and the logarithmic flux gains correspond exactly to the row of $[G_i]$ of those kinetic orders of independent variables in the synthesis term of this variable that are not affected by any other dependent variable. However, the only step in the pathway that can be unmodified by any dependent variable is the first step, in which the substrate is an independent variable, because the substrates of all other reactions are dependent variables. This implies that in a linear pathway in which none of the dependent variables inside this linear pathway is a modifier of the first step, the logarithmic flux gains of the pathway correspond exactly to the kinetic orders of the first reaction. In such cases, it is justified to

substitute the linear chain of reactions with one step in which the kinetic orders correspond to those of the first reaction. This procedure applies to v_{den}, v_{polyam}, and v_{trans}.

The kinetic orders for the S-system model were computed with Eq. (6), using the previous estimates of GMA kinetic orders and the values of fluxes at the operating point.

Applying these methods to published experimental data, we estimated the kinetic orders for every reaction of the pathway. The results are given in Appendix A following the order of the pathway of Fig. 1. The resulting kinetic orders of the GMA and S-system models are shown in Tables 4 and 5 respectively, the GMA rate constant and V_{vivo} are given in Table 6, and S-system rate constants are given in Table 7.

4. Preliminary model evaluation

4.1. Steady-state features

With 18 variables, 37 fluxes, and numerous modulations, the proposed models of purine metabolism are quite complicated, and a full evaluation is beyond our scope here. A rather detailed analysis of the steady-state properties can be found elsewhere [19]. This analysis demonstrates that the steady state is stable

Table 4
Values of GMA kinetic orders in alphabetical order

$f_{ada4} = 0.97$	$f_{ade6} = 0.55$	$f_{adrnr4} = 0.1$	$f_{adrnr9} = -0.3$
$f_{adrnr10} = 0.87$	$f_{ampd4} = 0.8$	$f_{ampd8} = -0.03$	$f_{ampd18} = -0.1$
$f_{aprt1} = 0.5$	$f_{aprt4} = -0.8$	$f_{aprt6} = 0.75$	$f_{asuc2} = 0.4$
$f_{asuc4} = -0.24$	$f_{asuc8} = 0.2$	$f_{asuc18} = -0.05$	$f_{asli3} = 0.99$
$f_{asli4} = -0.95$	$f_{dada9} = 1$	$f_{den1} = 2$	$f_{den2} = -0.06$
$f_{den4} = -0.25$	$f_{den8} = -0.2$	$f_{den18} = -0.08$	$f_{dgnuc10} = 1$
$f_{dnan12} = 1$	$f_{dnap9} = 0.42$	$f_{dnap10} = 0.33$	$f_{gdrnr8} = 0.4$
$f_{gdrnr9} = -1.2$	$f_{gdrnr10} = -0.39$	$f_{gmpr2} = -0.15$	$f_{gmpr4} = -0.07$
$f_{gmpr7} = -0.76$	$f_{gmpr8} = 0.7$	$f_{gmps4} = 0.12$	$f_{gmps7} = 0.16$
$f_{gnuc8} = 0.9$	$f_{gnuc18} = -0.34$	$f_{gprt1} = 1.2$	$f_{gprt8} = -1.2$
$f_{gprt15} = 0.42$	$f_{gua15} = 0.5$	$f_{hprt1} = 1.1$	$f_{hprt2} = -0.89$
$f_{hprt13} = 0.48$	$f_{hx13} = 1.12$	$f_{hxd13} = 0.65$	$f_{impd2} = 0.15$
$f_{impd7} = -0.09$	$f_{impd8} = -0.03$	$f_{inuc2} = 0.8$	$f_{inuc18} = -0.36$
$f_{mat4} = 0.2$	$f_{mat5} = -0.6$	$f_{polyam5} = 0.9$	$f_{prpps1} = -0.03$
$f_{prpps4} = -0.45$	$f_{prpps8} = -0.04$	$f_{prpps17} = 0.65$	$f_{prpps18} = 0.7$
$f_{pyr1} = 1.27$	$f_{rnan11} = 1$	$f_{rnap4} = 0.05$	$f_{rnap8} = 0.13$
$f_{trans5} = 0.33$	$f_{ua16} = 2.21$	$f_{x14} = 2.0$	$f_{xd14} = 0.55$

It should be noted that the kinetic order f_{dnan12} applies to v_{dnaa} and v_{dnag}, kinetic orders f_{dnap9} and f_{dnap10} apply to v_{adna} and v_{gdna}, the kinetic order f_{rnan11} applies to v_{rnaa} and v_{rnag}, and kinetic orders f_{rnap4} and f_{rnap8} apply to v_{arna} and v_{grna}. Further details are given in text and Appendix A.

Table 5
Values of the S-system kinetic orders (kinetic orders not presented in this table have a value of 0)

$g_{1,1} = -0.03$	$g_{1,4} = -0.45$	$g_{1,8} = -0.04$	$g_{1,17} = 0.65$	$g_{1,18} = 0.7$
$g_{2,1} = 0.720$	$g_{2,2} = -0.28$	$g_{2,4} = 0.319$	$g_{2,7} = -0.03$	$g_{2,8} = -0.02$
$g_{2,13} = 0.144$	$g_{2,18} = -0.06$	$g_{3,2} = 0.4$	$g_{3,4} = -0.24$	$g_{3,8} = 0.2$
$g_{3,18} = -0.05$	$g_{4,1} = 0.0002$	$g_{4,3} = 0.003$	$g_{4,4} = 0.0042$	$g_{4,5} = 0.002$
$g_{4,6} = 0.0003$	$g_{4,11} = 0.988$	$g_{5,4} = 0.2$	$g_{5,5} = -0.6$	$g_{6,5} = 0.9$
$g_{7,2} = 0.15$	$g_{7,7} = -0.09$	$g_{7,8} = -0.03$	$g_{8,1} = 0.003$	$g_{8,4} = 0.00014$
$g_{8,7} = 0.00019$	$g_{8,8} = -0.00335$	$g_{8,11} = 0.996$	$g_{8,15} = 0.001$	$g_{9,4} = 0.001$
$g_{9,9} = -0.0058$	$g_{9,10} = 0.017$	$g_{9,12} = 0.98$	$g_{10,8} = 0.005$	$g_{10,9} = -0.017$
$g_{10,10} = -0.006$	$g_{10,12} = 0.985$	$g_{11,4} = 0.05$	$g_{11,8} = 0.13$	$g_{12,9} = 0.42$
$g_{12,10} = 0.33$	$g_{13,2} = 0.43$	$g_{13,4} = 0.409$	$g_{13,9} = 0.04$	$g_{13,18} = -0.19$
$g_{14,13} = 0.343$	$g_{14,15} = 0.236$	$g_{15,8} = 0.881$	$g_{15,10} = 0.02$	$g_{15,18} = -0.33$
$g_{16,14} = 0.55$	$h_{1,1} = 1.27$	$h_{1,2} = -0.16$	$h_{1,4} = -0.06$	$h_{1,6} = 0.036$
$h_{1,8} = -0.23$	$h_{1,13} = 0.085$	$h_{1,15} = 0.074$	$h_{1,18} = -0.0092$	$h_{2,2} = 0.454$
$h_{2,4} = -0.15$	$h_{2,7} = -0.01$	$h_{2,8} = 0.126$	$h_{2,18} = -0.11$	$h_{3,3} = 0.99$
$h_{3,4} = -0.95$	$h_{4,4} = 0.054$	$h_{4,5} = -0.0045$	$h_{4,8} = 0.128$	$h_{4,9} = -2 \times 10^{-4}$
$h_{4,10} = 8 \times 10^{-5}$	$h_{4,18} = -0.0002$	$h_{5,5} = 0.368$	$h_{6,1} = 0.495$	$h_{6,4} = -0.79$
$h_{6,6} = 0.748$	$h_{7,4} = 0.12$	$h_{7,7} = 0.16$	$h_{8,2} = -5 \times 10^{-5}$	$h_{8,4} = 0.049$
$h_{8,7} = -0.0002$	$h_{8,8} = 0.132$	$h_{8,9} = -9 \times 10^{-5}$	$h_{8,10} = -2 \times 10^{-5}$	$h_{8,18} = -0.001$
$h_{9,9} = 0.431$	$h_{9,10} = 0.323$	$h_{10,9} = 0.413$	$h_{10,10} = 0.339$	$h_{11,11} = 1$
$h_{12,12} = 1$	$h_{13,1} = 0.817$	$h_{13,2} = -0.66$	$h_{13,13} = 0.528$	$h_{14,14} = 0.568$
$h_{15,1} = 0.925$	$h_{15,8} = -0.925$	$h_{15,15} = 0.438$	$h_{16,16} = 2.21$	

Table 6
Values of rate constants in GMA and V_{vivo} in CMM for each reaction, in alphabetical order

$\alpha_{ada} = 0.001062$	$\alpha_{ade} = 0.01$	$\alpha_{adna} = 3.2789$	$\alpha_{adrnr} = 0.0602$
$V_{vivo\ (ada)} = 86.1$	$V_{vivo\ (ade)} = 0.01$	$V_{vivo\ (adna)} = 35.7912$	$V_{vivo\ (adrnr)} = 0.1461$
$\alpha_{ampd} = 0.02688$	$\alpha_{aprt} = 233.8$	$\alpha_{arna} = 614.5$	$\alpha_{asuc} = 3.5932$
$V_{vivo\ (ampd)} = 33.4657$	$V_{vivo\ (aprt)} = 1045.64$	$V_{vivo\ (arna)} = 2414.63$	$V_{vivo\ (asuc)} = 37.7716$
$\alpha_{asli} = 66544$	$\alpha_{dada} = 0.03333$	$\alpha_{den} = 5.2728$	$\alpha_{dgnuc} = 0.03333$
$V_{vivo\ (asli)} = 1636.12$	$V_{vivo\ (dada)} = 79.3667$	$V_{vivo\ (den)} = 1278.32$	$V_{vivo\ (dgnuc)} = 3300.4$
$\alpha_{dnaa} = 0.001938$	$\alpha_{dnag} = 0.001318$	$\alpha_{gdna} = 2.2296$	$\alpha_{gdrnr} = 0.1199$
$V_{vivo\ (dnaa)} = 0.00194$	$V_{vivo\ (dnag)} = 0.001318$	$V_{vivo\ (gdna)} = 24.338$	$V_{vivo\ (gdrnr)} = 2.1963$
$\alpha_{gmpr} = 0.3005$	$\alpha_{gmps} = 0.3738$	$\alpha_{gnuc} = 0.2511$	$\alpha_{gprt} = 361.69$
$V_{vivo\ (gmpr)} = 0.3005$	$V_{vivo\ (gmps)} = 0.7483$	$V_{vivo\ (gnuc)} = 1600.22$	$V_{vivo\ (gprt)} = 5601$
$\alpha_{grna} = 409.6$	$\alpha_{gua} = 0.4919$	$\alpha_{hprt} = 12.569$	$\alpha_{hx} = 0.003793$
$V_{vivo\ (grna)} = 1609.75$	$V_{vivo\ (gua)} = 2.2$	$V_{vivo\ (hprt)} = 370.646$	$V_{vivo\ (hx)} = 0.003793$
$\alpha_{hxd} = 0.2754$	$\alpha_{impd} = 1.2823$	$\alpha_{inuc} = 0.9135$	$\alpha_{mat} = 7.2067$
$V_{vivo\ (hxd)} = 3.51428$	$V_{vivo\ (impd)} = 2.299$	$V_{vivo\ (inuc)} = 181.849$	$V_{vivo\ (mat)} = 42.6228$
$\alpha_{polyam} = 0.29$	$\alpha_{prpps} = 0.9$	$\alpha_{pyr} = 1.2951$	$\alpha_{rnaa} = 0.06923$
$V_{vivo\ (polyam)} = 13.635$	$V_{vivo\ (prpps)} = 16.7$	$V_{vivo\ (pyr)} = 1.2951$	$V_{vivo\ (rnaa)} = 0.06923$
$\alpha_{rnag} = 0.04615$	$\alpha_{trans} = 8.8539$	$\alpha_{ua} = 0.00008744$	$\alpha_{x} = 0.0012$
$V_{vivo\ (rnag)} = 0.04615$	$V_{vivo\ (trans)} = 20.985$	$V_{vivo\ (ua)} = 0.0000874$	$V_{vivo\ (x)} = 0.0012$
$\alpha_{xd} = 0.949$			
$V_{vivo\ (xd)} = 5.1106$			

Table 7
Values of rate constants in the S-system model

	Alpha	Beta
X_1	0.9	30.8182
X_2	1.6914	5.6
X_3	3.5932	66 544.7
X_4	0.08115	612.1
X_5	7.2067	9.001
X_6	0.29	223.54
X_7	1.2823	0.3738
X_8	0.0484	408.86
X_9	0.00227	3.3
X_{10}	0.00151	2.2629
X_{11}	1024.12	0.1154
X_{12}	5.5085	0.00325
X_{13}	0.10582	8.2073
X_{14}	0.7203	0.9324
X_{15}	0.26646	135.46
X_{16}	0.949	0.00008744

and quite robust. It is rather insensitive to changes in independent variables and parameters, but responsive enough to deal with physiological perturbations. Most of the over 1000 parameter sensitivities are less than one in magnitude, and among the remaining sensitivities, most are between 1 and 5, predicting that a 1% alteration in a parameter value would lead to a 1–5% change in the response variable. The relatively few sensitivities that are somewhat higher fall into two categories. Some are associated with the enzyme PPRPS, which is known to be crucial for the dynamics of purine metabolism; these higher sensitivities are thus a correct reflection of a well-known fact. A few are associated with marginal metabolites like HX, and therefore rather inconsequential. The generally low parameter sensitivities are important for another reason: they imply that inaccuracies in the estimation of parameter values have relatively minor consequences.

It may be noteworthy to comment on the quite complex stoichiometry of the model. Of course, at the steady state, the totality of inputs must equal the totality of outputs, and the equations indeed reflect this balance of fluxes. The stoichiometry is complicated, because key metabolites are composed of three different moieties, namely the purine ring, ribose, and phosphate. In numerous steps of the pathway, one of these moieties is either attached or split off, and this complicates any graphical representation. In order to keep confusion to a minimum, we decided to omit phosphate moieties from the pathway diagram and focus on ribose and the purine ring (see Fig. 1). This simplification does not affect the mathematical equations or any of the analyses. The equations

account for the dynamics of the relevant moieties through their mathematical structure and the values of their parameters.

Influxes of ribose and purine rings, respectively, occur in two places. The v_{prpps} step is the point of entry for the ribose moiety, while the v_{den} step represents entry of the purine ring. The two moieties leave the system in several processes. The ribose moiety is removed directly through the steps v_{pyr}, v_{polyam}, and indirectly through the steps v_{ada}, v_{dada}, v_{gnuc}, v_{dgnuc}, and v_{inuc}. The latter steps do not involve the loss of ribose directly, but are followed by splitting steps that occur within aggregated metabolite pools directly downstream. These reactions are catalyzed by purine nucleoside phosphorylase and separate the ribose moiety from the purine base. Purine rings leave the system through the steps v_{ade}, v_{hx}, v_{x}, and v_{ua}. As mentioned above, phosphate moieties are attached or removed in a large number of steps and even within pools.

4.2. Dynamic features

For the present evaluation, the three models (CMM, GMA, and S-system) are tested for consistency through simulations that reflect normal and pathological perturbations of purine metabolism. In particular, the purpose of the analysis is to determine whether one, two, or all three models yielded reasonable results, as measured against some representative biochemical and clinical observations.

Michaelis–Menten models are often considered the standard, and they have been the cornerstone of kinetic analyses in vitro for almost a century. Nonetheless, there is growing suspicion about whether these models are adequate in vivo [39,40]. It is not guaranteed that their underlying steady-state assumptions are satisfied in vivo. Relaxing the assumption of homogeneity leads to rate laws of different types [41]. Michaelis–Menten models of moderately sized pathways become rather intractable when it comes to mathematical analysis. Savageau [13] discussed the drastically increasing complexity of traditional rate laws, if they are affected by several modulators. Even analyses of essential features of pathways, such as steady states and their stability and sensitivities, become forbidding in Michaelis–Menten models of realistic, integrated pathways, while they are readily executed in power-law models. In the present case, we found it impossible to design a pure Michaelis–Menten model from existing data and had to complement it with power-law processes. These theoretical and practical concerns make the exploration of alternative models highly desirable.

Power-law models, whether of GMA, S-system, or Half-system type [9], have significant advantages when it comes to steady-state and dynamical analysis. The issue of potential concern here is that these models are developed as local representations of the actual rate law, which implies that their accuracy and reliability are guaranteed mathematically only for small perturbations. Even without this mathematical guarantee though, there is mounting empirical

evidence that power-law models often provide reliable representations for quite large ranges of variation in substrates or modulators. These ranges sometimes span several orders of magnitude [42–44]. Supporting and explaining these observations, Savageau [40,41,45] collated several direct studies and theoretical considerations [46–50] suggesting that power-law functions seem to be simple, yet adequate descriptions of processes in vivo.

It has been demonstrated several times that power-law models exhibit responses very similar to Michaelis–Menten equations, if the metabolites remain within ranges of physiological variation (e.g. Refs. [14,51]). However, it is difficult to assess in general how the three models compare under pathological conditions, as they are encountered in total or severe enzyme deficiencies. While one could argue that such conditions should be modeled at different operating points, one would consider it an advantage if the same numerical model could adequately represent both physiological and pathological conditions.

Three representative conditions were simulated: a 10-fold increase in PRPP; PRPPS superactivity; and HGPRT deficiency. The first simulation typifies a rather large, but still physiological deviation from the normal operating point. The second condition represents a persistent alteration in one of the key enzymes of purine metabolism. Clinically, this situation is accompanied by an overproduction of UA and gout. Mathematically, it is implemented as a two-fold increase in the activity of the first enzyme of the pathway, PRPPS (cf. Fig. 1). Such an increase is outside the typical range for which local approximations are guaranteed, even though power-law models have accurately modeled other phenomena of a similar type and magnitude of variation. The third situation exemplifies a drastic change in metabolism. Clinically, HGPRT deficiency is characterized by overproduction of UA and gout and, depending on the severity of the deficiency, by spasticity, choreoathetosis, mental retardation and self-mutilation, a symptom complex that is often referred to as Lesch–Nyhan syndrome [52]. Mathematically, the deficiency is implemented by decreasing the enzyme activity 100-fold. Such a deviation is far beyond the range of local deviation, and thus constitutes a test for the models outside the mathematically guaranteed range.

4.3. Simulation of a 10-fold increase in PRPP

For this type of simulation, the models are initiated with all metabolites at their physiological steady-state level. At time t_0, the concentration of PRPP is raised to a 10-fold increased value, and the models are solved numerically to show the dynamics of the metabolic system. Representative results of this set of simulations are shown in Fig. 2. Even though the concentration of PRPP is rather drastically increased by a factor 10, the three models seem to reflect the effects consistently. After a strong initial response (e.g., as shown in

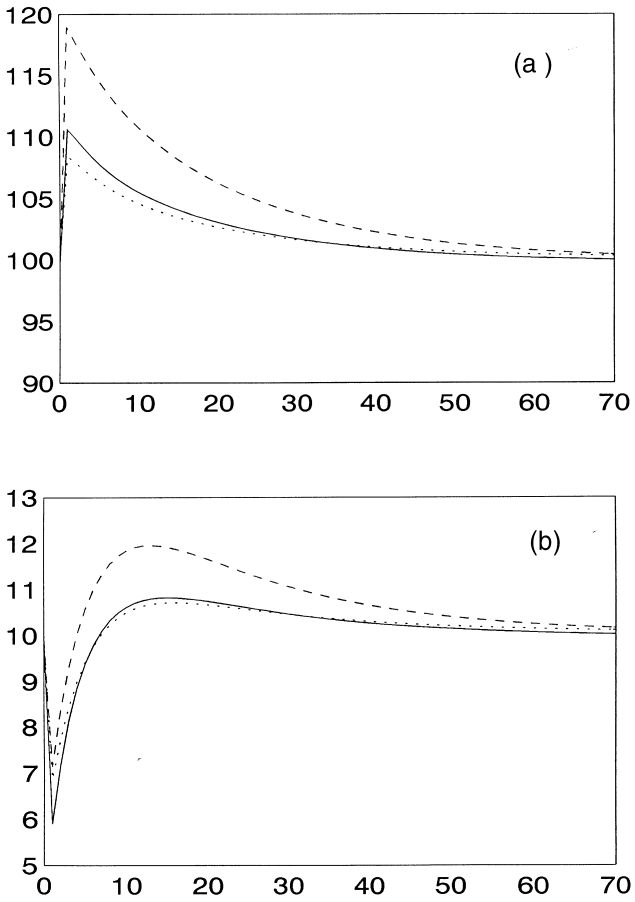

Fig. 2. Dynamic responses to a 10-fold increase in PRPP. At $t = 10$, PRPP was changed from 5 to 50 μM. Solid lines show predictions of the CMM model, dashed lines predictions of the GMA model, and dotted lines predictions of the S-system model. (a) Dynamic response of IMP (X_2). (b) Dynamic response of hypoxanthine (X_{13}).

Fig. 2 for IMP and HX), the system returns to the original, normal steady state.

Fig. 2 demonstrates that all three models have similar characteristics. In accord with earlier studies [14], the responses of the S-system and CMM models resemble each other more than those of the GMA and CMM models, but the differences may not be significant.

Other simulations of this type were executed and produced similar results. This suggests that the three models show similar dynamics as long as the perturbations are within a physiological range. There are no clinical data with

Table 8
Predictions of concentration and flux values in a simulation of PRPPS superactivity with the three models (units are (μM) for concentrations and (μM min^{-1} BW^{-1}) for fluxes)

Variables	Operational point	PRPPS superactivity				
		GMA	S-system	CMM	Clinical	Reference
PRPP	5	7.8	7.8	8.2	13–29	[79]
v_{den}	2.39	4.7	– [a]	4.8	4.7–12.4	[79]
X_{13} (not HX)	10	41	47	90	30	[74]
X_{14} or Xa	5	15	15	18	10	[74]
UA	100	131	132	126	300	[74]

[a] The flux of v_{den} cannot be obtained from the S-system model since it is part of the aggregated flux of PRPP degradation and IMP synthesis.

which to compare these dynamic responses quantitatively, but all observed system behaviors appear to be reasonable.

4.4. Simulation of PRPPS superactivity

To simulate PRPPS superactivity, V_{vivo} in the CMM model and the rate constants in the power-law models (GMA and S-system) were increased twofold. Some representative results are shown in Table 8, along with clinical observations. Since in this case a parameter value is changed, as opposed to an initial value in the previous set of simulations, the models assume new steady states. Again, results from the three models are quite similar, with the two power-law models being essentially indistinguishable. The results of all three models appear to be supported by the few available clinical observations. This is interesting to note, since the three models are based on different types of approximations and underlying assumptions. Also noteworthy is the fact that the issue of aggregation, which is the landmark distinction between GMA and S-system models, is inconsequential, even though the deviation from the operating point is extensive.

4.5. Simulation of severe HGPRT deficiency

HGPRT deficiency was modeled by reducing the activity of the enzyme to 1%. This was achieved by a 100-fold decrease in V_{vivo} for CMM and in the rate constants of v_{hprt} and v_{gprt} for GMA. In the S-system model the deficiency was simulated in two different ways: (i) by introducing the enzyme HGPRT as an independent variable of the model, and (ii) by multiplying the corresponding alphas and betas of the affected rate laws with the deficiency factor (0.01), raised to the aggregated kinetic order of the enzyme. As expected, both procedures yielded the same results.

Some representative simulation results from the three models are shown in Table 9, along with clinical measurements in Lesch–Nyhan patients. Also, critical fluxes are modeled by all three models with reasonable accuracy, as far as can be judged in comparison with clinical findings. However, some of the new steady-state values are unacceptable. In comparison with clinical observations, GMA performs better than either CMM or S-system. For instance, the CMM model overestimates the inosine concentration by about threefold and hypoxanthine excretion by 30-fold. The reasons for this are unclear. As pertains to the S-system, the aggregation apparently is no longer an appropriate procedure, and the S-system model breaks down, because of the large deviation from the operating point. This breakdown is not a structural all-or-nothing problem, but a gradual process, as is evident from simulations of mild HGPRT deficiencies, which are modeled with an accuracy similar to that in the PRPPS superactivity studies above (data not shown). In the case of severe HGPRT deficiency, the activity approaches very small values, and this has a strong impact on the aggregated product of power-law functions, thereby yielding the S-system representation unsatisfactory.

One can only speculate about the apparently good quality of the GMA model. Even though mathematically this is a local model, it seems to capture the dynamics of purine metabolism not just close to the chosen operating point, but over a very large range of conditions. Outside 'lucky coincidence', the first explanation that comes to mind is that the power-law representation of an individual reaction step or flux may indeed be a valid description of the process in nature, not just in a confined, approximate sense, but over the entire relevant

Table 9
Predictions of concentration and flux values in a simulation of HGPRT deficiency with the three models constructed (units are (μM) for concentrations and (μM min^{-1} BW^{-1}) for fluxes)

Variable	Operational point	HGPRT deficiency				
		GMA	S-system	CMM	Clinical	Reference
X_1 or PRPP	5	7.1	11.0	7.2	–	–
X_{13} (not HX)	10	70.6	1185.7	207	71	[80]
X_{14} or Xa	5	22.5	133.9	23	15	[80]
X_{15} (not Gua)	5	9	13.3	9.9	–	–
X_{16} or UA	100	145.7	226.6	129	150	[81]
v_{gua}	1.1	1.47	– [a]	1.5	–	–
v_{hxd}	1.23	4.4	– [a]	3.2	–	–
v_{xd}	2.3	5.3	14.0	4	7–14	[52]
v_{hx}	0.05	0.44	– [a]	1.5	0.45	[80]
v_x	0.03	0.6	– [a]	0.65	0.27	[80]
v_{ua}	2.3	5.3	14.0	4	7–14	[52]

[a] These non-aggregated fluxes cannot be obtained from the S-system model.

range of physiological and pathological variation. This explanation would be in line with measurements by Kohen et al. [48,49].

4.6. Issues of aggregation

Tables 8 and 9, and Fig. 2, demonstrate that the three models show similar results for small variations about the operating point, whereas they differ for large deviations. Previous comparisons between GMA, S-system and Michaelis–Menten rate laws had shown that S-system models generally agree with Michaelis–Menten models more closely than GMA models, if the metabolites and modulators remain within physiologically relevant ranges [14]. These earlier results are confirmed here for the complex and more realistic model of purine metabolism, as shown with the first two sets of simulations (Table 8 and Fig. 2).

For large variations, at least for those demonstrated here with the simulation of HGPRT deficiency, the S-system model appears to be inferior, predicting metabolite concentrations that are at variance with those observed clinically and predicted by CMM and GMA (Table 9). This discrepancy can be interpreted in two ways. On one hand, it is a consequence of violating the fundamental assumption of any Taylor approximation (which underlies the S-system model) that the variable of interest should not deviate from the operating point too much, lest the quality of approximation suffers. On the other hand, it can be seen as a direct result of the aggregation strategy that differentiates S-system and GMA.

To evaluate the latter, let us recall the definitions of the S-system parameters in Eq. (6). This equation shows that the aggregated parameters in S-systems are composed of kinetic orders of GMA (f_{i_r}), which can be expected to remain constant from one steady state to another, and of fluxes (v_{i_r} and v_{i_s}) which actually change from one steady state to another. An example is the S-system model parameter $h_{14,14}$ which in fact is a function of two GMA kinetic orders and two fluxes

$$h_{14,14} = \frac{f_{xd14} v_{xd} + f_{x14} v_x}{v_{xd} + v_x}.$$

In order to calculate the new values of $h_{14,14}$ in the S-system, we need actual flux values of v_{xd} and v_{x}. The S-system structure directly provides the value of v_{xd} which is equivalent to the synthesis of UA, but it does not provide the value of v_{x} because it is aggregated with v_{xd} into the degradation of Xa. To circumvent this problem, we introduce an ancillary variable (X_{19}) which collects the fraction of xanthine that is degraded via the excretory pathway v_{x} and that, in turn, is degraded by only one step (v_{ex}). v_{x} is characterized by the same kinetic parameters as before, and the parameters of v_{ex} are chosen to balance the degradation of the new variable and its synthesis: $f_{\mathrm{ex19}} = 0.5$ and $\alpha_{\mathrm{ex}} = 0.009486$. As to be expected, the introduction of the new variable did

not change any other property of the model but allowed us to evaluate the flux of v_x in the S-system simulations.

The values of the kinetic orders used for the computation of $h_{14,14}$ can be found in Table 4, and values of the fluxes at the operating point in Table 3. These values lead to the S-system parameter $h_{14,14} = 0.568$. However, when we alter the model, the values of v_{xd} and v_x may change, and so does $h_{14,14}$. For instance, the S-system simulation of PRPPS superactivity implies a value of $v_x = 0.2832$ which, together with the flux $v_{xd} = 4.2643$ and the kinetic orders in Table 4 results in $h_{14,14} = 0.6403$, a value which is close to the value (0.568) estimated at the operating point. In contrast, simulation of HGPRT deficiency with the S-system model yields $v_x = 21.5$ which, together with the flux $v_{xd} = 14$ and kinetic orders of Table 4, yields $h_{14,14} = 1.43$, a value three times higher than the value estimated at the operating point. This difference is directly responsible for the large concentration of xanthine that is predicted by the S-system model. The same argument (for the kinetic order $h_{13,13}$) explains the large and unphysiological accumulation of HX predicted by the S-system model for HGPRT deficient subjects (data not shown).

The case of HGPRT deficiency also demonstrates that the inaccuracy in the flux stoichiometry of S-system models can become significant for large deviations from the operating point. For example, we find $v_x = 21.5$ and $v_{xd} = 14.0$, whereas the flux of degradation of Xa is only 15.1. In the case of PRPPS superactivity, by contrast, the corresponding values in the S-system model are $v_x = 0.2832$ and $v_{xd} = 4.2643$, and the flux of degradation of Xa is 4.4113, which is reasonably consistent even for the 200% increase in the activity of PRPPS.

The GMA kinetic orders (f) also depend on the chosen operating point, and their values are determined by the steady state of the system. Similarly, the kinetic parameters (K_M) in the CMM model are 'apparent' K_Ms, and their values can vary with different conditions of the system in vivo. It is difficult to assess how strongly GMA or CMM parameters are affected by such changes. The GMA model, and to a lesser degree the CMM model, produces results that are quite similar to those measured in patients. Nevertheless, only one pathway is analyzed here, and further experimental and theoretical work is necessary to evaluate the reliability of these models in vivo.

Within the class of power-law models, S-system models have advantages when it comes to algebraic analysis. They are unique with respect to steady-state analysis [13] and optimization [53] and provide convenient tools for qualitative analysis [54]. For moderate variations about the operating point, their accuracy is usually sufficient. Their lack of accuracy in modeling situations such as severe HGPRT deficiency can be argued by asserting that an HGPRT deficient subject constitutes a metabolic system that is vastly different from normal, and that a new operating point should be selected for modeling such disorder. After all, a normal subject does not gradually become HGPRT deficient. We tested this hypothesis by using the same S-system model for both normal

and HGPRT deficient subjects and adjusting the parameter values to either one of the two steady states. As in the case of normal subjects, the S-system, the GMA, and the CMM models indeed produced very similar results for perturbations about the HGPRT deficient steady state (not shown). For instance, all three modeled perturbations in PRPP in a Lesch–Nyhan patient in a quantitatively similar fashion.

5. Discussion

This paper served two purposes. The first part was dedicated to screening the literature and extracting kinetic information that is necessary for any mathematical modeling of purine metabolism. This quite laborious exercise comprise both a conceptualization of the target system, which yield a scheme of metabolic relationships and regulatory signals, and an exhaustive search of relevant data. This process has been presented in detail so that future research can build upon it and replace current knowledge with new or fine-tuned results.

A large amount of material was collated, of which most is presented in Appendix A. This material is considered an important contribution, since it is useful not only for reproducing our results but also for designing other models of this pathway. There is no doubt that much is unknown about the biochemistry of purine metabolism, and as new data become available, they can be gradually incorporated into the parameter estimates presented here. Thus, the first part of this paper is largely independent of a particular modeling framework, even though we concentrated on standard procedures of traditional enzyme kinetics and more modern methods of BST. Nonetheless, other modeling approaches would require similar kinetic data.

The second part served the purpose of selecting a model for further analysis. While not shown, this was a several-year process involving numerous model revisions and refinements (for a detailed account, see Ref. [19]). At each stage, the current model was tested for consistency, stability, and robustness, and specific refinements were implemented to alleviate former problems. These refinements were usually introductions of fluxes or variables that had been assumed secondary in previous versions. Particular care was applied to these refinements, in order to assure biological validity and relevance.

In this process, the analytical tools developed in BST, specially the computation of parameter sensitivities and steady-state stability conditions, were fundamental in identifying potential unrealistic assumptions in the model. While it was not the purpose of this paper to provide detailed information about the process of designing the model, the process in itself revealed which variables affect the global behavior of the model most significantly. For example, the inclusion of SAM, RNA and DNA turned out to be the key to improving the robustness of the model. Accounting for excretion of purines (v_{ade}, v_{hx}, and

v_x) became critical, as it prevented the unphysiological accumulation of purine bases in several situations. By contrast, the addition of the flux v_{pyr} turned out to be almost inconsequential.

As in any modeling effort, we had to make several assumptions. The most critical are the following:

(i) The metabolites inside each pool were considered to be in equilibrium. Even though there is no real equilibrium between ATP and ADP (or other pairs of adenylates), there is experimental evidence that the energy charge is fairly constant under different physiological conditions. This suggested to consider ATP and ADP as if they were in equilibrium.

(ii) Several linear chains of reactions were lumped into single processes (e.g., v_{den}, v_{polyam}, and v_{trans}). This appeared to be legitimate, since it was demonstrated that the properties of the linear chain are closely related to those of the first step.

(iii) For this first analysis, we ignored the physiological compartmentalization of the human body. This was done to avoid overwhelming complexity, but it is clear that the consequences of this simplification should be analyzed. Because at the level of the whole human body, this assumption seems more risky. However, it should be seen as a conceptual election so that we can approach the analysis of purine metabolism as an integrated process. From the knowledge gained following this strategy, further improvement could include different compartments to produce a more realistic model.

Once a conceptual model was stablished, the challenge is to build up a mathematical model that allow us: (i) to validate the conceptual model; (ii) to discuss the system properties; and (iii) to predict specific features of the target metabolic pathway. The election of a particular framework for obtaining such a model is a difficult task. As a traditional standard, we attempted to develop a Michaelis–Menten model. However, this was not possible in a pure form, since some necessary information was simply not available in terms of kinetic parameters which are the characteristic elements for these types of models. Where possible (about half the time), reactions were formulated as kinetic rate laws of Michaelis–Menten type, and these were complemented with power-law kinetics in order to obtain a useable simulation tool. The lack of information, and the fact that our reactional scheme included different processes that were not single enzyme reactions but a pool of different processes, suggested the use of modeling strategies specifically devised for dealing with these situations. The S-system and GMA variants within BST were specially suited for this case.

Two types of power-law models were developed within the framework of BST. The kinetic parameters for these models were either derived from kinetic data in vitro or directly from experimental concentration and flux data and other qualitative information. The possibility of deriving useful estimation of the desired kinetic data from these assumption is one of the advantages of the modeling strategies in BST. Furthermore, the possibility of testing the mod-

el sensitivity towards any of the considered parameters is a valuable help for checking how critical is the choice of a particular parameter value from qualitative assumptions. The resulting GMA and S-system models are robust to parameter variation, so that the system properties would not significantly change with a slightly different choice in the parameter values.

For relatively small variations in metabolites or in model structure, all three models behaved quite similarly, and all results appeared to be reasonable and in accord with biochemical and clinical findings. The permissible ranges of deviation from normal operating conditions appeared to be wide enough to cover all physiological and mildly pathological conditions.

As one can see in Tables 8 and 9 for severe pathological conditions, the GMA model produced reasonable results, even if the system deviated far from the operating range. This observation is quite amazing, since the GMA model is based on local approximation. The GMA structure seems to cover a wide range of physiological and pathological conditions with one and the same numerical model, which was derived almost without further assumptions and exclusively from published data. Outside serendipity, a cautious explanation of this result may be that, for all practical purposes, metabolic processes in vivo follow power-law kinetics.

The results in Tables 8 and 9 are not only important for future decisions about model selection in similar situations, but they are biochemically important in themselves. For example, Table 9 suggests the investigation of some consequences of HGPRT deficiency that may not have been documented in the literature, such as increases in Gua and in the fluxes v_{gua} and v_{hxd}. Some of these issues are discussed elsewhere, but it is clear that models of the documented complexity will require further extensive experimental and mathematical evaluation.

Acknowledgements

This work was supported in part by a Grant from the Fondo de Investigaciones Sanitarias de la Seguridad Social (FISss 94/0860), and in part supported by a grant from The Upjohn Company. R. Curto was funded, as a Ph.D. student, by CIRIT BQF92.

Appendix A

A.1. Estimates of kinetic parameters for each reaction of the pathway

v_{prpps}: R5P + ATP $\rightarrow$ PRPP + AMP

PRPP (X_1) inhibits its own formation. According to Ref. [82], PRPP in a concentration of 1 mM inhibits v_{prpps} at 19%. Thus, $\text{PRPP}^{f_{\text{prpps1}}} = 1 - 0.19$ and $f_{\text{prpps1}} = -0.03$.

Ref. [82] also asserts that AMP and ADP in a concentration of 1 mM inhibit the reaction at 53% and 92%, respectively. Applying the procedure shown above, we obtain $f_{\text{prpps,AMP}} = -0.1$ and $f_{\text{prpps,ADP}} = -0.36$. Finally, ATP is a co-substrate of this reaction with a K_M that is higher than 14 μM. Derivation and normalization of Eq. (2), using this K_M and the corresponding steady-state concentration for ATP (see Table 1), implies that $f_{\text{prpps,ATP}} = 14/(14 + 1900) = 0.007$. As was explained before, f_{prpps4} is the sum of all kinetic orders associated with metabolites that constitute X_4: $f_{\text{prpps4}} = -0.45$.

Metabolites of the guanylate pool also inhibit this reaction. Ref. [82] found that 1 mM of GMP or GDP inhibits the reaction at 3% or 24%, respectively. Thus, $f_{\text{prpps,GMP}} = -0.004$, $f_{\text{prpps,GDP}} = -0.04$, and $f_{\text{prpps8}} = -0.04$.

According to Ref. [83], the apparent K_M for phosphate is 3.3 mM, and this yields $f_{\text{prpps18}} = 0.7$.

With $K_M = 33$ μM for R5P, [69,84], the kinetic equation for v_{prpps} reads

$$v_{\text{prpps}} = \frac{V_{\text{VIVO(PRPPS)}}\, X_{17}}{K_M + X_{17}} X_1^{f_{\text{prpps1}}} X_4^{f_{\text{prpps4}}} X_8^{f_{\text{prpps8}}} X_{18}^{f_{\text{prpps18}}}.$$

v_{den}:

As explained in the text, the parameters of this step can be estimated from the rate law of the first enzyme of the de novo pathway, which is amidophosphoribosyltransferase. The reaction catalyzed by this enzyme is

$$\text{PRPP} + \text{glutamine} + \text{H}_2\text{O} \rightarrow \beta\text{-5-phosphoribosyl-1-amine} + \text{glutamic acid} + \text{PPi}.$$

This reaction exhibits cooperative kinetics with respect to the substrate PRPP. According to Ref. [85], the K_M of PRPP varies between 140 and 480 μM, and the Hill coefficient (n) between 2 and 3, depending on the tissue. We selected the values $K_M = 300$ and $n = 2.2$.

Ref. [86] demonstrated that GMP, GDP and GTP in a concentration of 5 mM inhibit the reaction at 70%, 40% and 13%, respectively. This implies $f_{\text{den,GMP}} = -0.1413$, $f_{\text{den,GDP}} = -0.06$, and $f_{\text{den,GTP}} = -0.016$. Adding these values yields $f_{\text{den8}} = -0.2$.

Constituents of the adenylate pool also affect the reaction: AMP, ADP and ATP inhibit at 76%, 40% and 21%, respectively [86]. These results suggest $f_{\text{den,AMP}} = -0.1675$, $f_{\text{den,ADP}} = -0.06$, and $f_{\text{den,ATP}} = -0.028$, which yields essentially $f_{\text{den4}} = -0.25$.

5 mM IMP inhibits the reaction at 41% [86]. This yields $f_{\text{den2}} = -0.06$.

Ref. [87] showed that Pi inhibits v_{den} by changing the Hill coefficient of PRPP for this kinetics, taking the values of Hill coefficients reported at 0,

25, and 50 mM, one obtains the strength of inhibition of Pi at these concentrations, which suggests $f_{\text{den18}} = -0.08$.

Summarizing these data, we obtain the complete kinetic rate law

$$v_{\text{den}} = \frac{V_{\text{VIVO(DEN)}}\, X_1^n}{K_M + X_1^n}\, X_2^{f_{\text{den2}}}\, X_4^{f_{\text{den4}}}\, X_8^{f_{\text{den8}}}\, X_{18}^{f_{\text{den18}}}.$$

v_{gprt}: Gua + PRPP → GMP + PPi

This enzyme is reversible. However, it is thought that the enzyme in vivo only catalyzes the reaction in the direction indicated above. To account for these uncertainties, we considered the reaction as essentially irreversible, but allowed for inhibition by the product GMP. The kinetic rate law was thus represented as suggested by Ref. [88]

$$v_{\text{gprt}} = \frac{V_{\text{VIVO(GPRT)}}\left(\text{AB} - \text{PQ}\frac{K_{\text{iA}}K_{\text{iB}}}{K_{\text{iP}}K_{\text{iQ}}}\right)}{K_{\text{B}}K_{\text{iA}} + \text{A}K_{\text{B}} + \text{B}K_{\text{A}} + \text{AB} + \text{P}\frac{K_{\text{iA}}K_{\text{B}}}{K_{\text{iP}}} + \text{Q}\frac{K_{\text{B}}K_{\text{iA}}}{K_{\text{iQ}}} + \text{PQ}\frac{K_{\text{iA}}K_{\text{B}}}{K_{\text{iQ}}K_{\text{P}}} + \left(\text{ABP}\frac{1}{K_{\text{iP}}}\right) + \text{BPQ}\frac{K_{\text{A}}}{K_{\text{iQ}}K_{\text{P}}} + \text{AP}\frac{K_{\text{B}}}{K_{\text{iP}}} + \text{BQ}\frac{K_{\text{A}}}{K_{\text{iQ}}}}.$$

In this formulation, A, B, P, and Q code for PRPP, Gua, Pyrophosphate and GMP, respectively. Their concentrations were estimated at the operating point. For pyrophosphate, the concentration was set as 15 μM [89], and the K_{A}, K_{B}, K_{iP}, and K_{iQ} were set as 240, 4, 2100, and 1.25 μM. The remaining three parameters, K_{P}, K_{iA} and K_{iB} could not be estimated from data. However, it turned out that K_{P} has almost no influence on the system (results not shown), and we selected a value of $K_{\text{P}} = 1000$ μM. K_{iA} and K_{iB} are the inhibition constants of PRPP and Gua, respectively. These again had little effect on the results, and we selected values of K_{iA} and $K_{\text{iB}} = 4$ and 1 μM, respectively, which are close to the concentrations of the associated metabolites.

v_{hprt}: HX + PRPP → PPi + IMP

This reaction and the v_{gprt} reaction are catalyzed by the same enzyme, hypoxanthine-guanine phosphoribosyltransferase (HGPRT). The same questions about reversibility apply, and they are handled in the same fashion. An appropriate rate law, according to Ref. [90], is

$$v_{\text{hprt}} = \frac{V_{\text{VIVO(HPRT)}}\left(AB - \frac{V_f K_{\text{iB}}K_{\text{A}}}{V_f K_{\text{iQ}}K_{\text{P}}}PQ\right)}{\frac{K_{\text{iB}}K_{\text{A}}}{K_{\text{iA}}K_{\text{iQ}}K_{\text{P}}}\text{APQ} + \frac{K_{\text{iB}}K_{\text{A}}}{K_{\text{iQ}}K_{\text{P}}}\text{PQ} + \frac{K_{\text{B}}}{K_{\text{iP}}}\text{AP} + \frac{K_{\text{B}}}{K_{\text{iQ}}}\text{QA} + \text{AB} + \frac{K_{\text{iB}}K_{\text{A}}}{K_{\text{iP}}}\text{P} + \frac{K_{\text{iB}}K_{\text{A}}}{K_{\text{iQ}}}\text{Q} + K_{\text{B}}\text{A} + K_{\text{A}}\text{B} + K_{\text{A}}K_{\text{iB}}}.$$

The symbols A, B, P, and Q represent HX, PRPP, IMP and Pyrophosphate, respectively, and the constants K_{A}, K_{B}, K_{P}, K_{Q}, K_{iB}, K_{iP}, K_{iQ} are 7.7, 66, 5.8, 39, 25, 40, and 260 μM. The constant K_{iA} has not been experimentally determined. However, because model evaluations demonstrate that outputs are

practically unaffected when the parameter K_{iA} is varied between 1 and 200, we used a $K_{iA} = 10$ μM [1] and a concentration of 15 μM for PPi [89].

v_{aprt}: Ade + PRPP → AMP + PPi

This enzyme is similar in type to hypoxanthine-guanine phosphoribosyltransferase. It also could possibly catalyze a reversible reaction, although the reverse reaction seems irrelevant in vivo. To account for this uncertainty, inhibition of the product AMP has been included.

The substrate PRPP has a K_M close to 6 μM [29,91,92], and we select $K_M = 5$ μM.

The K_M for Ade has values between 1.1 and 5.2 μM [29,91,92]. This implies $f_{aprt,Ade}$ between 0.5 and 0.83, and we set $f_{aprt6} = 0.75$.

The K_i for AMP is between 7.5 and 30 μM [29,93]. Inhibition is competitive with respect to PRPP, and this suggests that $f_{aprt,AMP}$ should range between −0.76 and −0.96. Selecting $f_{aprt4} = -0.8$, we obtain the rate law

$$v_{aprt} = \frac{V_{VIVO(APRT)}\, X_1}{X_1 + K_M}\, X_6^{f_{aprt6}}\, X_4^{f_{aprt4}}.$$

v_{pyr}:

Because the initial enzyme in the synthesis of pyrimidines is also a phosphoribosyltransferase, it seems reasonable to assume that its kinetic parameters are similar to those of v_{hprt}, v_{gprt} or v_{aprt}. We roughly estimated the value of f_{pyr1} as an average of f_{gprt1}, f_{hprt1}, and f_{aprt1}, which yielded $f_{pyr1} = 1.27$. It is shown elsewhere [19] that sensitivities of variables to this parameter have low values. The kinetic properties of this step are reflected in the power function rate law

$$v_{pyr} = \alpha_{pyr}\, X_1^{f_{pyr1}}.$$

v_{impd}: IMP + NAD + H_2O → XMP + NADH

Ref. [94] published a table of K_M values for this enzyme in different tissues: for example, in Yoshida tumor cells 12 μM, in human placenta 14 μM, and in human leukemia cells 23 μM. For our model, we chose an average value of $K_M = 17$.

XMP and GMP inhibit the enzyme by competing with IMP. The K_i for XMP is 25 μM and for GMP it is 90 μM [94,95]. The kinetic rate law for competitive inhibition suggests $f_{impd,GMP} = -0.03$ and, thus, $f_{impd8} = -0.03$.

$$v_{impd} = \frac{V_{VIVO(IMPD)} X_2}{K_M\left(1 + X_7 \frac{1}{K_{I(XMP)}}\right) + X_2}\, X_8^{f_{impd8}}.$$

v_{gmps}: XMP + ATP + glutamine → GMP + AMP + PPi + glutamate

The published value of $K_M = 270$ μM for ATP [96] suggests the parameter value $f_{gmps4} = 0.12$. Moreover, the K_M for XMP is 4.9 μM [96], which yields the kinetic equation

$$v_{\text{gmps}} = \frac{V_{\text{VIVO(GMPS)}}\, X_7}{X_7 + K_M}\, X_4^{f_{\text{gmps4}}}.$$

v_{asuc}: IMP + L-aspartate + GTP $\rightarrow$ S-AMP + GDP + Pi

The enzyme comes in the form of two isoenzymes (L and M) that have different kinetic characteristics [97]. A rigorous assessment of the contributions of each isozyme is difficult, and we use an average of $K_M = 66.6$ [97,98]. GTP and Asp are cosubstrates for this reaction. Aspartate is not included in the model, but an average K_M for GTP [97,98] suggests $f_{\text{asuc,GTP}} = 0.2$, and thus $f_{\text{asuc8}} = 0.2$.

Adenylates in general, and AMP in particular inhibit this reaction competitively with respect to IMP. Using a K_{i} value of 170 μM for AMP and a K_M of 37 μM for IMP [98] in the traditional rate law for competitive inhibition, one obtains $f_{\text{asuc,AMP}} = -0.24$ and, thus, $f_{\text{asuc4}} = -0.24$.

Finally, Pi in concentrations of 2 or 20 mM inhibits the enzyme at 20% and 59%, respectively [99]. This is represented with the parameter setting $f_{\text{asuc18}} = -0.05$.

Summarizing these results, an appropriate rate law is

$$v_{\text{asuc}} = \frac{V_{\text{VIVO(ASUC)}}\, X_2}{K_M + X_2}\, X_4^{f_{\text{asuc4}}}\, X_8^{f_{\text{asuc8}}}\, X_{18}^{f_{\text{asuc18}}}.$$

v_{asli}:

This enzyme catalyzes two reactions of purine metabolism. One of them, the reaction of v_{asli}, is specifically depicted in Fig. 1.

S-AMP $\rightarrow$ AMP + fumarate

AMP acts as a competitive inhibitor of the enzyme with a K_{i} of 9.2 μM for AMP [100]. With $K_M = 1.79$ μM for S-AMP [100], the appropriate kinetic rate law is

$$v_{\text{asli}} = \frac{\mathrm{V}_{\text{VIVO(ASLI)}}\, X_3}{K_M\left(1 + X_4 \frac{0.08}{K_{\text{I}}}\right) + X_3}.$$

The second reaction constitutes one of the steps in the ten step pathway of de novo purine synthesis (v_{den}). This reaction is rather insignificant, and we do not consider it here.

v_{gmpr}: GMP + NADPH $\leftrightarrow$ IMP + NADP + NH_3

The substrate GMP has a K_M of 7.5 μM [101], which corresponds to $f_{\text{gmpr,GMP}} = 0.23$. This effect of a guanylate is augmented by the activation of the enzyme by GDP and GTP. 2 μM of GTP or GDP activate the enzyme at 22% or 13%, respectively [101]. Thus, $f_{\text{gmpr,GTP}} = 0.29$ and $f_{\text{gmpr,GDP}} = 0.18$ which, added to $f_{\text{gmpr,GMP}}$, yields $f_{\text{gmpr8}} = 0.7$. XMP is a potent inhibitor of the enzyme: 33 μM of XMP inhibit the enzyme at 93% [102]. This is represented with the setting $f_{\text{gmpr7}} = -0.76$.

v_{gmpr} is a reversible step, in which the product (IMP) inhibits the enzyme. IMP in a concentration of 33 μM inhibits the enzyme at 30%, and 330 μM inhibits at 70% [102], which suggests a value for f_{gmpr2} between −0.1 and −0.2. We use the average $f_{\text{gmpr2}} = -0.15$.

Adenylates inhibit the enzyme less strongly than guanylates. In a concentration of 33 μM, AMP inhibits the enzyme at 5%, ADP at 7% and ATP at 11% [102]. This implies $f_{\text{gmpr,AMP}} = -0.01$; $f_{\text{gmpr,ADP}} = -0.02$, $f_{\text{gmpr,ATP}} = -0.04$, and $f_{\text{gmpr4}} = -0.07$.

The kinetic rate law of this reaction in power-law form is thus

$$v_{\text{gmpr}} = \alpha_{\text{gmpr}} X_2^{f_{\text{gmpr2}}} X_4^{f_{\text{gmpr4}}} X_7^{f_{\text{gmpr7}}} X_8^{f_{\text{gmpr8}}}.$$

v_{ampd}: AMP → IMP + NH_3

This enzyme exhibits cooperativity with respect to its substrate AMP. This suggests a Hill rate law whose parameters are appropriately chosen as $K_M = 2300$ μM and $n = 1.4$ [103–106]. GTP inhibits the enzyme, thereby affecting the apparent K_M and n [105]. The result is a smaller reaction rate with an approximate kinetic order $f_{\text{ampd8}} = -0.03$.

Pi is an inhibitor of this enzyme with a K_i of 16 mM in human kidney [106]. 2.5 mM of Pi decrease the flux from 24.79 to 13.71 in human heart [105], and 1.8 mM inhibit the reaction in human erythrocytes by 50% [104]. These data correspond to kinetic orders of f_{ampd18} of −0.08, −0.075, and −0.1, respectively, and we specify the parameter as $f_{\text{ampd18}} = -0.1$.

The appropriate kinetic rate law is thus

$$v_{\text{ampd}} = \frac{V_{\text{VIVO(AMPD)}} (X_4\ 0.08)^n}{K_M + (X_4\ 0.08)^n} X_8^{f_{\text{ampd8}}} X_{18}^{f_{\text{ampd18}}}.$$

v_{mat}: methionine + ATP → SAM + Pi + PPi

The K_M of this enzyme for ATP is 450 μM [63]. The enzyme is inhibited uncompetitively by SAM with a K_i between 2 and 2.9 μM [63], which suggests a kinetic order of $f_{\text{mat5}} = -0.6$. The kinetic rate law is thus

$$v_{\text{mat}} = \frac{V_{\text{VIVO(MAT)}}\ X_4\ 0.76}{X_4\ 0.76 + K_M} X_5^{f_{\text{mat5}}}.$$

v_{trans}: protein + SAM → methylated protein + S-adenosyl-L-homocysteine

For this transmethylation pathway we use the kinetic parameters of the first enzyme (protein carboxyl methyl transferase) which has a K_M for SAM of 2 μM [63,107]. This yields the following rate law:

$$v_{\text{trans}} = \frac{V_{\text{VIVO(TRANS)}}\ X_5}{K_M + X_5}.$$

v_{polyam}:

This pathway, like v_{den} and v_{trans}, includes several enzymes. As discussed before, it is justified to use the kinetics of the first enzyme in the pathway (S-adenosyl-methionine decarboxylase) which catalyzes the step

SAM $\rightarrow$ decarboxilated SAM

Decarboxylated SAM is subsequently transformed into 5-methylthioadenosine, which in turn is the substrate for the linear polyamine pathway that eventually produces Ade. The K_M of SAM decarboxylase for SAM is 50 μM [108]. This yields the kinetic rate law

$$v_{\text{polyam}} = \frac{V_{\text{VIVO(POLYAM)}}\, X_5}{K_M + X_5}.$$

v_{inuc}: IMP + H_2O $\rightarrow$ Ino + Pi

There is a large variety of 5′-nucleotidases. Among them, the 5′-nucleotidases (E.C. 3.1.3.5.) hydrolyze nucleotides to nucleosides with some residual activity for hydrolyzing deoxynucleotides. Others (5′(3′)-nucleotidases E.C.3.1.3.31.) hydrolyze deoxynucleotides to deoxynucleosides with some residual activity for hydrolyzing nucleotides. The nucleotidases determine the kinetic parameters v_{inuc}, v_{gnuc}, and v_{dgnuc}. Among the 5′-nucleotidases, several subkinds need to be distinguished. The ecto 5′-nucleotidases have a high specificity for AMP and a lesser specificity for IMP and GMP, whereas the cytosolic 5′-nucleotidases have a higher specificity for IMP and GMP. For our purposes, we focussed on the kinetic parameters of the more relevant cytosolic 5′-nucleotidase-II for v_{inuc} and v_{gnuc} [109]. Assuming a Michaelis–Menten mechanism, the values of K_M of this enzyme for IMP are somewhat higher than 400 μM [109–111].

Pi is an inhibitor of the enzyme: 1 mM Pi increases the K_M from 200 to 4800 μM, [111], which corresponds to a concomitant tenfold decrease in the flux rate, thus suggesting $f_{\text{inuc18}} = -0.36$. Based on these experimental data, the appropriate kinetic rate law is

$$v_{\text{inuc}} = \frac{V_{\text{VIVO(INUC)}}\, X_2}{K_M + X_2}\, X_{18}^{f_{\text{inuc18}}}.$$

v_{gnuc}: GMP + H_2O $\rightarrow$ Guo + Pi

For this enzyme we also assume a Michaelis–Menten mechanism with the kinetic parameters of cytosolic 5′-nucleotidase-II. Data [109–111] suggest a K_M for GMP of about 700 μM.

Pi inhibits this enzyme, changing the K_M from 700 to 7900 μM [111]. The appropriate kinetic order is $f_{\text{gnuc18}} = -0.34$, and the resulting rate law is

$$v_{\text{gnuc}} = \frac{V_{\text{VIVO(GNUC)}}\, X_8\, 0.0625}{X_8\, 0.0625 + K_M}\, X_{18}^{f_{\text{gnuc18}}}.$$

v_{dgnuc}: dGMP + H_2O → dGuo + Pi

Again, we assume a Michaelis–Menten mechanism with kinetic parameters for 5′(3′)-nucleotidases, because it seems that this enzyme catalyzes the reaction in vivo. The K_M of this enzyme for dGMP is very high, with a value over 3.3 mM [112]. This yields the following rate law:

$$v_{\text{dgnuc}} = \frac{V_{\text{VIVO(DGNUC)}}\, X_{10}\, 0.0333}{K_M + X_{10}\, 0.0333}.$$

v_{gdrnr}: GDP + NADPH → dGDP + NADP + H_2O

Diribonucleotide reductase is an allosteric enzyme that is modulated by deoxynucleotides. There are different kinds of this enzyme, but the human enzyme is in the same class with that of other mammals and of *E.coli*. The estimation of kinetic orders was based on data from calf thymus [113].

The K_M of this enzyme for GDP is 50 μM [113]. dATP is a potent inhibitor of this reaction, but its kinetic order is difficult to estimate. We used the equation $f_{\text{gdrnr,dATP}} = \text{d}(\log v_{\text{gdrnr}})/\text{d}([\text{dATP}])\,[\text{dATP}]_0$ to estimate it, and with numerical values obtained from [113], we obtained the kinetic order $f_{\text{gdrnr9}} = -1.2$.

Similarly, dGTP is an inhibitor whose kinetic order is difficult to estimate. Again using data from the study by Ref. [113], we graphed the logarithm of v_{gdrnr} against the logarithm of the concentration [dGTP]. After removing obvious outliers, the slope of the regression line was −0.39, with a correlation coefficient of 0.9999. Hence, $f_{\text{gdrnr10}} = -0.39$.

The appropriate kinetic rate law is

$$v_{\text{gdrnr}} = \frac{V_{\text{VIVO(GDRNR)}}\, X_8\, 0.1875}{K_M + X_8\, 0.1875}\, X_9^{f_{\text{gdrnr9}}}\, X_{10}^{f_{\text{gdrnr10}}}.$$

v_{adrnr}: ADP + NADPH → dADP + NADP + H_2O

The same enzyme catalyzes v_{adrnr} and v_{gdrnr}, but the kinetics of the reactions differ quite significantly. According to Ref. [113], the K_M for ADP is about 44 μM. 5 μM of dATP inhibits v_{adrnr} at 50% [113], and this produces an approximate kinetic order of $f_{\text{adrnr9}} = -0.3$.

dGTP in this case acts as an activator of the reaction. Its kinetic order was estimated from Ref. [113] as $f_{\text{adrnr,dGTP}} = \text{d}(\log\ v_{\text{adrnr}})/\text{d}(\log\ [\text{dGTP}]) = 0.87$. Thus, $f_{\text{adrnr10}} = 0.87$.

The resulting rate law is

$$v_{\text{adrnr}} = \frac{V_{\text{VIVO(ADRNR)}}\, X_4\, 0.16}{X_4\, 0.16 + K_M}\, X_9^{f_{\text{adrnr9}}}\, X_{10}^{f_{\text{adrnr10}}}.$$

v_{ada}: Ado → Ino + NH_3

Adenosine deaminase (ADA) is an irreversible enzyme that catalyzes the deamination of Ado to Ino and of dAdo to dIno. The enzyme apparently is ubiquitous in all species and tissues, with K_M's for Ado in humans that range

between 17 and 100 μM [30,31,114]. We selected a value of $K_M = 20$ μM for the following rate law:

$$v_{\text{ada}} = \frac{V_{\text{VIVO(ADA)}}\, X_4\, 0.0002}{X_4\, 0.0002 + K_M}.$$

v_{dada}: dAdo → dIno + NH_3

This reaction is also catalyzed by ADA, with a K_M for dAdo of 38 μM [114]. This yields the rate law

$$v_{\text{dada}} = \frac{V_{\text{VIVO(DADA)}}\, X_4\, 0.016}{X_4\, 0.016 + K_M}.$$

v_{arna} and v_{grna}:

The RNA nucleotidyltransferase adds nucleotides to the RNA strands, following the reaction

(ATP or GTP) + RNA_n → PPi + RNA_{n+1}

Because both fluxes produce essentially the same product, the kinetics of these fluxes are constrained to be the same except for their rate constants. Specifically, to preserve the stoichiometric composition of RNA, V_{VIVO} in v_{arna} must be $\frac{3}{2}$ times that in v_{grna}. Because the kinetic parameters of these two fluxes must be equal, the same kinetic orders f_{rnap4} and f_{rnap8} (referring to the formation of RNA by RNA polymerase) are used in the GMA rate law of the two reactions v_{arna} and v_{grna}. The K_Ms for ATP and GTP are 100 and 45 μM, respectively [115]. These data suffice to determine power-law kinetic orders, but as was commented in the text, power-law parameters are insufficient to determine Michaelis–Menten parameters. In this case we need to determine Michaelis–Menten parameters for a bisubstrate enzyme,

$$\frac{v_{\text{arna}}}{v_{\text{grna}}} \text{ or } = \text{ or } \frac{V_{\text{VIVO(ARNA)}}}{V_{\text{VIVO(GRNA)}}} \frac{X_4\, 0.76\, X_8\, 0.75}{K_M + K_A\, X_4\, 0.76 + K_G\, X_8\, 0.75 + K_C\, X_8\, 0.75\, X_4\, 0.76}.$$

We still have two degrees of freedom in determining the kinetic parameters of this reaction, so two additional constraints are needed, and we set K_M and $K_C = 1$ μM. With these specifications, we obtain the values $K_A = 47.5$ and $K_G = 115.9$.

v_{rnaa} and v_{rnag}:

Several enzymes hydrolyze nucleic acids to nucleotides and deoxynucleotides: 5′3′-exonucleases, 3′5′-exonucleases, endonucleases, H ribonuclease, and some other unspecific enzymes. The reactions, catalyzed by any of these enzymes, do not have exactly the same stoichiometry. Because the ratio Ade/Gua in RNA is constant, the kinetics of Ade and Gua must be equal, except in the values of their rate constants, as was the case for v_{arna} and v_{grna}. Here, the kinetic order representing the degradation of RNA is called f_{rnan11}. We

set the value for this kinetic order as $f_{\text{rnan11}} = 1$. This parameter is discussed elsewhere [19] in more detail, and it is sufficient to note here that changes in this parameter do not affect the behavior of the system much. The power function rate law for this step of the pathway is

$$\begin{array}{l} v_{\text{rnaa}}\ V_{\text{VIVO(RNAA)}} \\ \text{or} = \text{or}\ X_{11}^{f_{\text{rnan11}}}. \\ v_{\text{rnag}}\ V_{\text{VIVO(RNAG)}} \end{array}$$

v_{adna} and v_{gdna}: (dATP or dGTP) + $\text{DNA}_n \rightarrow$ PPi + DNA_{n+1}

This enzyme adds deoxynucleotides to DNA strands, and because the ratio of added dATP and dGTP is constrained by the structure of DNA, the corresponding rate law must be equal except for the rate constants, as was discussed in the preceding case. The kinetic orders used in the two reactions are called f_{dnap9} and f_{dnap10}. The K_Ms for dATP and dGTP are 3 and 1.2 μM, respectively [116]. Still, there are two degrees of freedom in the kinetic rate law for these bisubstrate reactions, and we set K_M and $K_C = 1$ μM. With these specifications, we obtain the parameter values $K_{\text{A}} = 2.58$ μM and $K_G = 5.54$ μM in the following rate law:

$$\begin{array}{l} v_{\text{adna}}\ V_{\text{VIVO(ADNA)}} \\ \text{or} = \text{or}\ \dfrac{X_9\ 0.66\ X_{10}\ 0.8}{K_M + K_A\ X_9\ 0.66 + K_G\ X_{10}\ 0.8 + K_C\ X_9\ 0.8\ X_{10}\ 0.66}. \\ v_{\text{gdna}}\ V_{\text{VIVO(GDNA)}} \end{array}$$

v_{dnaa} and v_{dnag}:

These two fluxes are constrained and pose the same estimation problems as the degradation of RNA (see above). We made the same assumptions, specifying $f_{\text{dnan12}} = 1$ for both kinetic rate laws. This parameter is discussed further in Ref. [19]. The rate law for this step is thus

$$\begin{array}{l} v_{\text{dnaa}}\ V_{\text{VIVO(DNAA)}} \\ \text{or} = \text{or}\ X_{11}^{f_{\text{dnan11}}}. \\ v_{\text{dnag}}\ V_{\text{VIVO(DNAG)}} \end{array}$$

v_{hxd}: HX + H_2O + (NAD or O_2) → Xa + (NADH or H_2O_2)

The conversion of HX to Xa and subsequently to UA is irreversibly catalyzed by the enzyme xanthine oxidase, if oxygen is used as the electron acceptor, or by xanthine dehydrogenase, if NAD is the electron acceptor. These two enzymatic activities are carried out by the same protein which can switch from one catalytic activity to the other. In humans, the two reactions take place only in liver and gut, and there is no agreement about which of the activities is more significant in vivo: Some references [33] purport that the main activity rests with xanthine dehydrogenase, while others [20] consider xanthine oxidase as more important in vivo. For our models, we set the K_M value of this enzyme with respect to HX as 13 μM (cf. [117]), which yields Michaelis–Menten reaction

$$v_{\text{hxd}} = \frac{V_{\text{VIVO(HXD)}}\, X_{13}\, 0.7}{X_{13}\, 0.7 + K_M}.$$

v_{xd}: Xa + H_2O + (NAD or O_2) → UA + (NADH or H_2O_2)

This reaction is catalyzed by the same enzyme as v_{hxd}. The K_Ms of the enzyme for Xa are 15.5 and 3 μM for human gut and human liver, respectively [118], and we set $K_M = 6$ μM in the Michaelis–Menten rate law

$$v_{\text{xd}} = \frac{V_{\text{VIVO(XD)}}\, X_{14}}{X_{14} + K_M}.$$

v_{gua}: Gua + H_2O → Xa + NH_3

Guanase or guanine aminohydrolase is believed to be a Michaelian enzyme with a K_M for the substrate Gua of 0.56 μM in human erythrocytes [57]. This value has been used for the Michaelis–Menten rate law

$$v_{\text{gua}} = \frac{V_{\text{VIVO(GUA)}}\, X_{15}\, 0.1}{X_{15}\, 0.1 + K_M}.$$

v_{ade}:

This flux represents the oxidation of Ade to 2,8-dihydroxyadenine and the excretion of this end product and of Ade in urine. When we take values measured in vivo [65] and plot the logarithm of adenine metabolite excretion against the logarithm of plasma adenine concentration (see Fig. 3(a)) we obtain a reasonably straight line with a slope equal to f_{ade6}. The kinetic order thus determined is $f_{\text{ade6}} = 0.55$, and the rate law is

$$v_{\text{ade}} = \alpha_{\text{ade}}\, X_6^{f_{\text{ade6}}}.$$

v_{hx}:

This flux represents excretion of HX in urine and is not an enzymatic rate. We can estimate its parameter values by solving a system of two equations. In every steady state these values have to satisfy the condition $v_{\text{hx}} = \alpha_{\text{hx}}\, X_{13}^{\text{fhx13}}$. Also, we know that at our operating point [HX] $= 7$ μM and $v_{\text{HX}} = 0.05$ μmol min^{-1} BW^{-1}. Furthermore, it is known that in Lesch–Nyhan patients [HX] is about 50 μM and v_{HX} is over 0.45 μM min^{-1} BW^{-1} [80]. Substitution of these data and solving the equations results in the kinetic order $f_{\text{hx13}} = 1.12$. The rate law thus is

$$v_{\text{hx}} = \alpha_{\text{hx}}\, X_{13}^{f_{\text{hx13}}}.$$

v_{x}:

This flux represents excretion of Xa in urine. As in the previous case of v_{hx}, its kinetic order has been determined from two equations at the operating point, one with Xa = 5 μM and $v_{\text{x}} = 0.03$ μmol min^{-1} BW^{-1} for healthy subjects, and the other with Xa of about 15 μM and v_{x} of about 0.27 μmol min^{-1} BW^{-1}

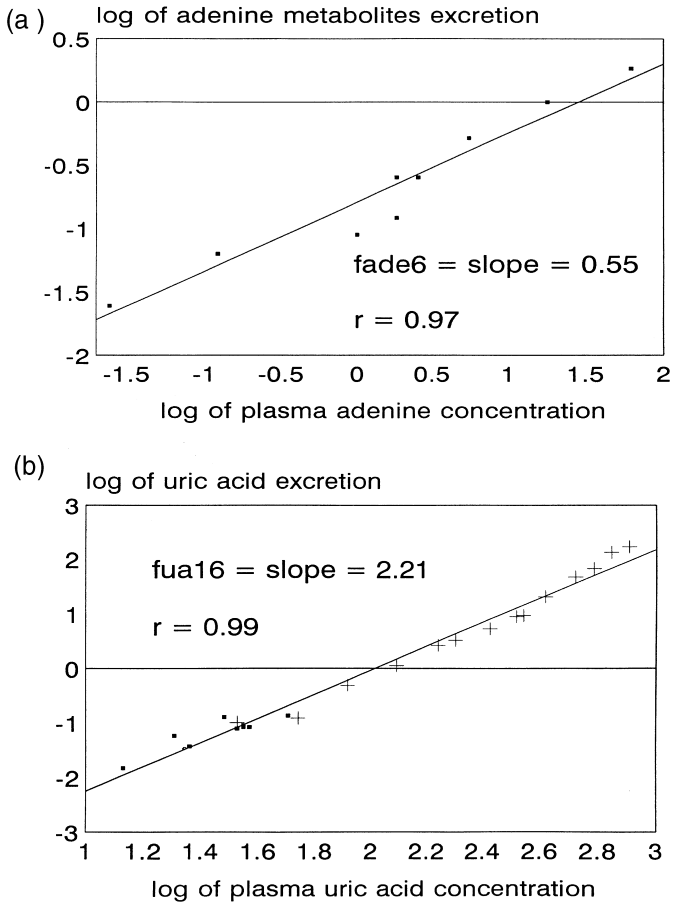

Fig. 3. Graphical representation of the regression for estimating f_{ade6} (panel a) and f_{ua16} (panel b) in healthy subjects. Symbols for panel b are: (■) measurements obtained from different individuals; (+) measurements from the same individual after injections of UA.

for Lesch–Nyhan patients [80]. With these data we obtain a kinetic order of $f_{x14} = 2$ and the rate law

$$v_x = \alpha_x X_{14}^{f_{x14}}.$$

v_{ua}:

This flux represents excretion of UA by the kidneys and gut. Again, this flux is not an enzyme catalyzed reaction, which made it impossible to find a kinetic rate law in the literature. However, as most UA is eliminated in urine, it has been possible to assess v_{ua} in vivo by measuring the concentration of UA in urine every day. The resulting data, as obtained from [119], were represented in a

log–log plot (Fig. 3(b)) in which the slope corresponds to f_{ua16}, with the numerical value $f_{\mathrm{ua16}} = 2.21$. The Y axis in this plot does not represent the logarithm of total concentration of UA in the human body, because these data were not available. Instead, it represents the logarithm of plasma UA concentration, which is assumed to be proportional to the total concentration in the human body, and thus leads to the same slope. The appropriate rate law is

$$v_{\mathrm{ua}} = \alpha_{\mathrm{ua}} X_{16}^{f_{\mathrm{ua16}}}.$$

We have demonstrated in this section how one can construct a CMM model from kinetic parameters and other information found in the literature. By showing almost all steps of estimation, this section can easily be extended, amended, or rectified as new data become available. The CMM estimates provided the basis for the pure power-law models in GMA and S-system form. To construct the GMA model, we applied Eq. (4) to the CMM rate laws for all fluxes. The resulting kinetic orders of the GMA model are shown in Table 4. Subsequent application of Eq. (6) to each process of synthesis or degradation then yielded the kinetic orders of the corresponding S-system model. These results are shown in Table 5.

A.2. Estimated values of rate constants and V_{vivo}

The last set of parameters that need to be estimated for the three models consists of rate constants in GMA and S-system and V_{vivo} in CMM. To estimate these parameters we need all previously determined parameter values, as well as the concentrations of all metabolites and the flux rates at the operating point. These pieces of information allow us to solve one equation for each rate law in which either the rate constant or V_{vivo} is the only unknown. Results for CMM and GMA models are given in Table 6, and results for the S-system model in Table 7.

References

[1] R. Franco, E.I. Canela, Computer simulation of purine metabolism, European J. Biochem. 144 (1984) 305.
[2] F. Heinmets, Supercomputer analysis of purine and pyrimidine metabolism leading to DNA-Synthesis, Cell Biophys. 14 (1989) 283.
[3] T. Bartel, H. Holzhütter, Mathematical modelling of the purine metabolism of the rat liver, Biochim. Biophys. Acta 1035 (1990) 331.
[4] P. Fritzson, Regulation of nucleotidase activities in animal tisues, Adv. Enzyme Regul. 16 (1978) 43.
[5] J.B. Pritchard, F. Chavez-Peon, R.D. Berlin, Purines: supply by liver to tissues., Am. J. Physiol. 219 (1970) 1263.
[6] R.A. Lewis, R.K. Haag, Purine nucleoside phosphorilase of bovine liver mithochondria, Adv. Exp. Med. Biol. B 309 (1991) 181.

[7] M.A. Savageau, Biochemical systems analysis. I. Some mathematical properties of the rate law for the component enzymatic reactions, J. Theoret. Biol. 25 (1969) 365.
[8] M.A. Savageau, Biochemical systems analysis II. Steady state solutions for an *n*-poll system using a power-law approximation, J. Theoret. Biol. 25 (1969) 370.
[9] E.O. Voit (Ed.), Canonical Nonlinear Modeling: S-system Approach to Understanding Complexity, Van Nostrand Reinhold, New York, 1991.
[10] R. Curto, A. Sorribas, M. Cascante, Comparative characterization of the fermentation pathway of Saccharomyces cerevisiae using biochemical systems theory and metabolic control analysis: model definition and nomenclature, Math. Biosci. 130 (1995) 25.
[11] M. Cascante, R. Curto, A. Sorribas, Comparative characterization of the fermentation pathway of saccharomyces cerevisiae using biochemical systems theory and metabolic control analysis: steady-state analysys, Math. Biosci. 130 (1995) 51.
[12] A. Sorribas, R. Curto, M. Cascante, Comparative characterization of the fermentation pathway of Saccharomyces cerevisiae using biochemical systems theory and metabolic control analysys: model validation and dynamic behaviour, Math. Biosci. 130 (1995) 71.
[13] M.A. Savageau, Biochemical systems analysis: a study of function and design in molecular biology, Addison-Wesley, Reading, MA, 1976.
[14] E.O. Voit, M.A. Savageau, Accuracy of alternative representations for integrated biochemical systems, Biochemistry 26 (1987) 6869.
[15] L. Michaelis, M.L. Menten, Die Kinetik der Invertinwirkung, Biochem. Z. 49 (1913) 333.
[16] M.A. Savageau, E.O. Voit, D.H. Irvine, Biochemical systems theory and metabolic control theory: 1. Fundamental similarities and differences, Math. Biosc. 86 (1987) 127.
[17] M.A. Savageau, E.O. Voit, D.H. Irvine, Biochemical systems theory and metabolic control theory: 2. The role of sumation and connectivity relationships, Math. Biosc. 86 (1987) 147.
[18] F.O. Hoffman, J.S. Hammonds, Propagation of uncertainty in risk assessments: the need to distinguish between uncertainty due to lack of knowledge and uncertainty due to variability, Risk Analysis 14 (5) (1994) 707.
[19] R. Curto, The usefulness of mathematical models in biotechnological and clinical studies: analysis of ethanolic fermentation pathway in Saccharomyces cerevisiae and purine metabolism in humans, Universitat de Barcelona, 1996.
[20] T.D. Palella, I.H. Fox, Hyperuricemia and gout in: C.R. Scriver, A.L. Beaudet, W.S. Sly, D. Valle (Ed.), The Metabolic Basis of Inherited Disease, McGraw-Hill, New York, 1989, p. 965.
[21] M.J. Bradford, I.H. Krakoff, R. Leeper, M.E. Balis, Study of purine metabolism in a xanthinuric female, J. Clin. Invest. 47 (1968) 1325.
[22] N.L. Edwards, D. Recker, I.H. Fox, Overproduction of uric acid in hypoxanthine-guanine phosphoribosyltransferase deficiency, J. Clin. Invest. 63 (1979) 922.
[23] T. Page, W.L. Nyhan, A.L. Yu, J. Yu, A syndrome of megaloblastic anemia, inmunodeficiency, and exesive nucleotide degradation, Adv. Exp. Med. Biol. 309B (1991) 345.
[24] J.H. Ayvazian, S. Skupp, The study of purine utilization and excretion in a xanthinuric man, J. Clin. Invest. 44 (1965) 1248.
[25] J.H. Ayvazian, S. Skupp, Study of the utilization and excretion of dietary purines in a xanthinuric man, J. Clin. Invest. 45 (1966) 1859.
[26] F.F. Snyder, J.F. Henderson, Alternative pathways of deoxyadenosine and adenosine metabolism, J. Biol. Chem. 248 (1973) 5899.
[27] M.S. Hershfield, J.E. Seegmiller, Regulation of de novo purine biosynthesis in human lymphoblasts, J. Biol. Chem. 251 (1976) 7348.
[28] K.J. Van Acker, H.A. Simonds, C. Potter, J.S. Cameron, Complete deficiency of adenine phosphoribosyltransferase, N. Engl. J. Med. 297 (1977) 127.
[29] H.A. Simmonds, A.S. Sahota, K.J. Van Acker, Adenine phosphoribosyltransferase deficiency and 2,8-dihydroxyadenine lithiasis, in: C.R. Scriver, A.L. Beaudet, W.S. Sly, D.

Valle (Eds.), The Metabolic Basis of Inherited Disease, McGraw-Hill, New York, 1989, p. 1029.
[30] J.D. Geiger, J.I. Nagy, Adenosine deaminase and [3H] nitrobenzylthioinosine as markers of adenosine metabolism and transport in central purinergic systems, in: M. Williams (Ed.), Adenosine and Adenosine Receptors, Humanae Press, Clifton, New Jersey, 1990, p. 225.
[31] N.M. Kredich, M.S. Hersfield, Immunodeficiency diseases caused by adenosine deaminase deficiency and Purine nucleoside phosphorylase deficiency, in: C.R. Scriver, A.L. Beaudet, W.S. Sly, D. Valle (Ed.), The Metabolic Basis of Inherited Disease, McGraw-Hill, New York, 1989, p. 1045.
[32] F. Bontemps, G. Van den Berghe, H.G. Hers, Evidence for a substrate cycle between AMP and adenosine in isolated hepatocytes, Proc. Natl. Acad. Sci. USA 80 (1983) 2829.
[33] E.W. Holmes, J.B. Wyngaarden, Hereditary xanthinuria, in: C.R. Scriver, A.L. Beaudet, W.S. Sly, D. Valle (Ed.), The Metabolic Basis of Inherited Disease, McGraw-Hill, New York, 1989, p. 1085.
[34] H. Kather, Pathways of purine metabolism in human adipocytes – Further evidence against a role of adenosine as an endogenous regulator of human fat-cell function, J. Biol. Chem. 265 (1990) 96.
[35] H.R. Horton, L.A. Moran, R.S. Ochs, J.D. Rawn, K.G. Scrimgeour, Transcription and the Processing of RNA, in: H.R. Horton, L.A. Moran, R.S. Ochs, J.D. Rawn, K.G. Scrimgeour (Ed.), Principles of Biochemistry, Prentice-Hall, New Jersey, ch. 21, 1993.
[36] G. Sander, H. Topp, G. Heller-Schöch, J. Wieland, G. Schöch, Ribonucleic acid turnover in man: RNA catabolites in urine as measure for the metabolism of each of the three major species of RNA, Clin. Sci. 71 (1986) 367.
[37] M. Cascante, R. Franco, E.I. Canela, Sensitivity analysis. A common foundation of theories for the quantitative study of metabolic control, in: E.O. Voit (Ed.), Canonical Nonlinear Modeling. S-System Approach to Understanding Complexity, Van Nostrand Reinhold, New York, 1991, pp. 76.
[38] M.A. Savageau, A. Sorribas, Constraints among molecular and systemic properties – Implications for physiological genetics, J. Theoret. Biol. 141 (1989) 93.
[39] C.M. Hill, R.D. Waight, W.G. Bardsley, Does any enzyme follow the Michaelis–Menten equation?, Molec. Cell. Biochem. 15 (1977) 173.
[40] M.A. Savageau, Critique of the enzymologists test tube, in: E. Bittar (Ed.), Foundations of Medical Cell Biology, Jai Press, Greenwich, CT, 1992, pp. 45.
[41] M.A. Savageau, Michaelis–Menten mechanism reconsidered: implications of fractal kinetics, J. Theoret. Biol. 176 (1995) 115.
[42] Peschel, The Predator–Prey Model: Do We Live in a Volterra World? Akademie-Verlag, Berlin, 1986.
[43] M.A. Savageau, Cascaded enzymatic mechanisms in: M.A. Savageau (Ed.), Biochemical Systems Analysis: A Study of Function and Design in Molecular Biology, Addison-Wesley, London, 1976, p. 217.
[44] M.A. Savageau, Mechanisms of gene action, in: M.A. Savageau (Ed.), Biochemical Systems Analysis: A Study of Function and Design in Molecular Biology, Addison-Wesley, London, 1976, p. 235.
[45] M.A. Savageau, Enzyme kinetics in vitro and in vivo: Michaelis–Menten revisited, in: E.E. Bittar (Ed.), Principles of Medical Biology, Jai Press, Greenwich. Connecticut, 1995, p. 93.
[46] J.A. Roels, Energetics and Kinetics in Biotechnology, Elsevier, Amsterdam, 1983.
[47] J.S. Newhouse, R. Kopleman, Reaction kinetics on clusters and islands, J. Chem. Phys. 85 (1986) 6804.
[48] E. Kohen, C. Khoen, B. Thorell, G. Wagner, Quantitative aspects of rapid microfluorometry for the study of enzyme reactions and transport mechanisms in single living cells, in: A.A.

Thaer, M. Sernetz (Ed.), Fluorescence Techniches in Cell Biology, Springer, New York, 1973, p. 207.
[49] E. Kohen, B. Thorell, C. Khoen, J.M. Solmon, Studies of metabolic events in localized compartments of the living cell by rapid microspectro-fluorometry, Adv. Biol. Med. Phys. 15 (1974) 271.
[50] R. Kopleman, Rate processes on fractals: theory, simulations, and experiments, J. Statist. Phys. 42 (1986) 185.
[51] A. Sorribas, M.A. Savageau, A comparison of variant theories of intact biochemical systems. 2. Flux-oriented and metabolic control theories, Math. Biosci. 94 (1989) 195.
[52] J.E. Seegmiller, F.M. Rosenbloom, Enzyme defect associated with a sex-linked human neurological disorder and excesive purine synthesis, Science 155 (1967) 1682.
[53] E.O. Voit, Optimization in integrated biochemical systems, Biotechnol. Bioeng. 40 (1992) 572.
[54] D.C. Lewis, Qualitative analysis of S-systems: Hopf bifurcations, in: E.O. Voit (Ed.), Canonocal Nonlinear Modeling: S-System Approach to Understanding Complexity, Van Nostrand Reinhold, New York, 1991, p. 304.
[55] J.B. Wyngaarden, W.N. Kelley, Gout, in: J.B. Stanbury, J.B. Wyngaarden, D.S. Fredrickson, J.L. Goldstein, M.S. Brown (Ed.), The Metabolic Basis of Inherited Disease, McGraw-Hill, New York, 1983, p. 1043.
[56] N. Kamatani, S. Kuroshima, Ch. Terai, M. Hakoda, K. Nishioka, K. Mikanagi, Diagnosis of genotypes for AdeninePhosphoribosyltransferase (APRT) deficiency, Adv. Exp. Med. Biol. 253A (1989) 51.
[57] A. Giacomello, C. Salerno, Possible metabolic basis for GTP depletion in red cells of patients with PRPP synthetase superactivity, Adv. Exp. Med. Biol. 309B (1991) 253.
[58] K. Pillwein, P. Chiva, A. Knoflach, B. Czermak, K. Schuster, E. Gersdorf, B. Ausserer, C. Murr, R. Goebl, G. Stockhammer, H. Maier, H. Kostron, Purine metabolism of human glioblastoma invivo, Cancer Res. 50 (1990) 1576.
[59] M.N. Goodman, J.M. Lowenstein, The purine nucleotide cycle. Studies of ammonia production by skeletal muscle in situ and in perfused preparations, J. Biol. Chem. 252 (1977) 5054.
[60] W.G. Siems, T. Grune, R. Schmidt, R. Uhlig, G. Gerber, Y.V. Tikhonov, A.M. Pimenov, R.T. Toguzov, Purine nucleotides, nucleosides and nucleobases of liver, skeletal muscle, blood and tumor cells during the growth of Erlich Ascites tumor in mice, Adv. Exp. Med. Biol. 309A (1991) 113.
[61] T. Grune, W.G. Siems, G. Gerber, R. Uhlig, Determination of the ultraviolet absorbency and radioactivity of purine compounds separated by high-performance liquid-chromatography – Application to metabolic flux rate analysis, J. Chromatogr. 553 (1991) 193.
[62] J.R. Barber, B.H. Morimoto, L.S. Brunauer, S. Clarke, Metabolism of S-adenosyl-L-methionine in intact human erythrocytes, Biochim. Biophys. Acta 887 (1986) 361.
[63] K.L. Oden, S. Clarke, S-adenosyl-L-metionine synthase from human erythrocytes: role in the regulation of cellular S-adenosylmethionine levels, Biochemistry 22 (1983) 2978.
[64] T. Grune, W. Siems, R. Uhlig, P. Langen, G. Gerber, Changes of purine nucleotide metabolism of Erlich ascites cells during transition of tumor growth, Adv. Exp. Med. Biol. 309A (1991) 109.
[65] C.H. de Verdier, A. Ericson, F. Niklasson, M. Westman, Adenine metabolism in man. 1. After intravenous and preoral administration, Scand. J. Clin. Lab. Invest. 37 (1977) 567.
[66] A. Tabucchi, F. Carlucci, R. Pagani, F. Ciccomascolo, L. Lopalco, A. Siccardi, Some aspects of purine nucleotide metabolism in human lymphocytes: nucleotide content in human lymphoblastoid lines transfected with HIV-1, Adv. Exp. Med. Biol. 309A (1991) 121.
[67] G. Morgan, S. Strobel, C. Montero, J.A. Duley, P.M. Davies, H.A. Simmonds, Raised IMP-dehydrogenase activity in the erythrocytes of a case of purine nucleoside (PNP) deficiency, Adv. Exp. Med. Biol. 309B (1991) 297.

[68] J.G. Cory, Metabolismo de los nucleótidos purínicos y pirimidínicos, in: T.M. Devlin (Ed.), Bioquímica, Reverte S.A., Barcelona, 1988, p. 618.
[69] S. Kunjara, M. Sochor, A.L. Greenbaum, P. Mclean, Aspects of the regulation of hepatic phosphoribosyl pyrophosphate formation in the obese (ob/ob) mouse – Relationship to the pentose phosphate pathway, Biochem. Med. Metab. Biol. 49 (1993) 217.
[70] K.R. Albe, B.E. Wright, Carbohydrate metabolism in dictyostelium discoideum: II. Systems' Analysis, J. Theoret. Biol. 169 (1994) 243.
[71] L. Stryer. DNA y RNA: Las moléculas de la herencia, in: L. Stryer (Ed.), Bioquímica, Reverté S.A., Barcelona, 1988, p. 71.
[72] J.G. Puig, I.H. Fox, F.A. Mateos, M.L. Jimenez, Adenine-nucleotide turnover in hypoxanthine-guanine phosphoribosyl-transferase deficiency – Evidence for an increased contribution of purine biosynthesis de Novo, Metabolism 38 (1989) 410.
[73] M.E. King, J.M. Honeysett, S.B. Howell, Regulation of de novo purine synthesis in human bone marrow mononuclear cells by hypoxanthine, J. Clin. Invest. 72 (1983) 965.
[74] M.L. Jimenez, J.G. Puig, F.A. Mateos, T.H. Ramos, J.S. Melian, V.G. Nieto, M.A. Becker, Increased purine nucleotide degradation in the central nervous system (CNS) in PRPPS synthetase superactivity, Adv. Exp. Med. Biol. 253A (1989) 9.
[75] T.W. Traut, P.A. Ropp, A. Poma, Purine nucleoside phosphorylase: allosteric regulation of a dissociating enzyme, Adv. Exp. Med. Biol. 309B (1991) 177.
[76] E. Zoref-Shani, G. Kessler-Icekson, L. Wasserman, O. Sperling, Characterization of purine nucleotide metabolism in primary rat cardiomyocyte cultures, Biochim. Biophys. Acta 804 (1984) 161.
[77] J.M. Whelan, A.S. Bagnara, Factors affecting the rate of purine ribonucleotide dephosphorylation in human erythrocytes, Biochim. Biophys. Acta 563 (1979) 466.
[78] K.J. Van Acker, H.A. Simonds, Long-term evolution of type 1 Adenine phosphoribosyltransferase (APRT) deficiency, Adv. Exp. Med. Biol. 309B (1991) 91.
[79] M.A. Becker, J.G. Puig, F.A. Mateos, M.L. Jimenez, M. Kim, H.A. Simmonds, Neurodevelopmental impairment and deranged PRPP and purine nucleotide synthesisin inherited superactivity of PRPPsynthetase, Adv. Exp. Med. Biol. 253A (1989) 15.
[80] R.A. Harkness, Lesch–Nyhan syndrome: reduced aminoacid concentrations in CSF and brain, Adv. Exp. Med. Biol. 253A (1989) 159.
[81] S. Fujimori, T. Tagaya, N. Yamaoka, N. Kamatani, L. Akaoka, Molecular analysis of hypoxanthine-guanine phosphoribosyltransferase deficiency in Japanese patients, Adv. Exp. Med. Biol. 309B (1991) 101.
[82] I.H. Fox, W.N. Kelley, Human phosphoribosylpyrophosphate synthetase kinetic mechanism and end product inhibition, J. Biol. Chem. 247 (1972) 2126.
[83] I.H. Fox, W.N. Kelley, Human phosphoribosylpyrophosphte synthetase, distribution purification and properties, J. Biol. Chem. 246 (1971) 5739.
[84] P.A.M. Berman, L. Human, Regulation of 5-phosphoribosyl 1-pyrophosphate and of hypoxanthine uptake and release in human erythrocytes by oxypurine cycling, J. Biol. Chem. 265 (1990) 6562.
[85] E.W. Holmes, Kinetic, physical, and regulatory properties of amidophosphoribosyltransferase, Adv. Enzyme Regul. 19 (1981) 215.
[86] E.W. Holmes, J.A. McDonald, J.M. McCord, J.B. Wyngaarden, W.N. Kelley, Human glutamine phosphoribosylpyrophosphate amidotransferase. Kinetic and regulatory properties, J. Biol. Chem. 248 (1973) 144.
[87] J. Kovarsky, M.C. Evans, E.W. Holmes, Regulation of human amidophosphoribosyltransferase: interaction of ortophosphate, PP-ribose-P, and purine ribonucleotides, Canad. J. Biochem. 56 (1978) 334.
[88] J.F. Henderson, L.W. Brox, W.N. Kelley, F.M. Rosenbloom, J.E. Seegmiller, Kinetic studies of hypoxanthine-guanine phosphoribosyltransferase, J. Biol. Chem. 243 (1968) 2514.

[89] K.R. Albe, M.H. Butler, B.E. Wright, Cellular concentrations of enzymes and their substrates, J. Theoret. Biol. 143 (1990) 163.
[90] A. Giacomello, C. Salerno, Human hypoxanthine-guanine phosphoribosyltransferase, J. Biol. Chem. 253 (1978) 6038.
[91] H. Holmsen, M.C. Rozenberg, Adenine nucleotidemetabolism of blood platelets. III Adenine phosphoribosyl transferase and nucleotide formation from exogenous adenine, Biochim. Biophys. Acta 157 (1968) 266.
[92] S. Fujimori, I. Akaoka, K. Sakamoto, H. Yamanaka, K. Nishioka, N. Kamatani, Common characteristics of mutant adenine phosphoribosyltransferases from four separate Japanese families with 2,8-dihydroxyadenine urolithiasis associated with partial enzyme deficiencies., Hum. Genet. 71 (1985) 171.
[93] M. Hori, J.F. Henderson, Kinetic studies of adenine phosphoribosyltransferase, J. Biol. Chem. 241 (1966) 3404.
[94] M.E. Pugh, E.B. Skibo, Inosine monophosphate dehydrogenase from porcine (Sus-scrofa-domestica) thymus – Purification and properties, Comp. Biochem. Physiol. [B] 105 (1993) 381.
[95] E.W. Holmes, D.M. Pehlke, N. Kelley, Human IMP dehydrogenase kinetics and regulatory properties, Biochim. Biophys. Acta 364 (1974) 209.
[96] T. Page, B. Bakay, W.L. Nyhan, Human GMP synthetase, Int. J. Biochem. 16 (1984) 117.
[97] Y. Matsuda, H. Ogawa, S. Fukutome, H. Shiraki, H. Nakagawa, Adenylosuccinate synthetase in rat liver: the existence of two types and their regulatori roles, Biochem. Biophys. Res. Commun. 78 (1977) 766.
[98] M.B. Van der Weyden, W.N. Kelley, Human Adenilosuccinate Synthetase. Partial purification, kinetic and regulatory properties of the enzyme from placenta, J. Biol. Chem. 249 (1974) 7282.
[99] H. Ogawa, H. Shiraki, Y. Matsuda, K. Kakiuchi, H. Nakagawa, Purification, crystalization, and properties of adenylosuccinate synthetase from rat skelethal muscle, J. Biochem. 81 (1977) 859.
[100] R.L. Stone, H. Zalkin, J.E. Dixon, Expression, purification, and kinetic characterization of recombinant human adenylosuccinate lyase, J. Biol. Chem. 268 (1993) 19710.
[101] T. Spector, T.E. Jones, R.L. Miller, Reaction mechanism and specificity of human GMP reductase, J. Biol. Chem. 254 (1979) 2308.
[102] J.J. Mackenzie, L.B. Sorensen, Guanosine 5'-phosphate reductase of human erythrocytes, Biochim. Biophys. Acta 327 (1973) 282.
[103] G. Nagel-Starczynowska, G. Nowak, K. Kaletha, Purification and properties of AMP-deaminase from human uterine smooth-muscle, Biochim. Biophys. Acta 1073 (1991) 470.
[104] S. Yun, C.H. Suelter, Human erythrocyte 5'-AMP aminohydrolase purification and characterization, J. Biol. Chem. 253 (1978) 404.
[105] G. Nowak, K. Kaletha, Molecular-forms of human heart-muscle AMP deaminase, Biochem. Med. Metab. Biol. 46 (1991) 263.
[106] G. Nowak, K. Kaletha, Purification and properties of AMP-deaminase from human kidney, Biochem. Med. Metab. Biol. 47 (1992) 232.
[107] S. Clarke, Protein carboxyl methyltransferases: two distinct classes of enzymes, Ann. Rev. Biochem. 54 (1985) 479.
[108] A.E. Pegg, H.G. Williams-Ashman, On the role of S-adenosyl-L-methionoe in the biosynthesis of spermidine by rat prostate, J. Biol. Chem. 244 (1969) 682.
[109] H. Zimmermann, 5'- Nucleotidase: molecular estructure and functional aspects, Biochem. J. 285 (1992) 345.
[110] R. Itoh, J. Oka, Evidence for existence of a cytosol 5'-nucleotidase in chicken heart: comparision of some properties of heart and liver enzymes, Comp. Biochem. Physiol. 81B (1985) 159.

[111] R. Itoh, Purification and some properties of cytosol 5'-nucleotidase from rat liver, Biochim. Biophys. Acta 657 (1981) 402.
[112] L. Höglund, P. Reichard, Cytoplasmatic 5'(3')-nucleotidase from human placenta, J. Biol. Chem. 265 (1990) 6589.
[113] S. Eriksson, L. Thelander, M. Akerman, Allosteric regulation of calf thymus ribonucleoside diphosphate reductase, Biochemistry 18 (1979) 2948.
[114] P.D. Boyer, The binding change mechanism for ATP synthase – Some probabilities and possibilities, Biochim. Biophys. Acta 276 (1993) 257.
[115] P.L. Ballard, H.G. Williams-Ashman, Isolation and properties of a testicular ribonucleic acid polymerase, J. Biol. Chem. 241 (1966) 1602.
[116] P.A. Fisher, T.S. Wang, D. Korn, Enzymological Characterization of DNA Polymerase alpha, Basic catalytic properties, processivity, and GAP utilization of the homogeneous enzyme from human KB cells, J. Biol. Chem. 254 (1979) 6128.
[117] C.F. Strittmatter, Studies on avian xanthine dehydrogenases. Properties and patterns of appearance during development, J. Biol. Chem. 240 (1965) 2557.
[118] P.K. Bondy, L.E. Rosenberg, Duncan's Diseases of Metabolism, Saunders, Philadelphia, 1974.
[119] W. Lathem, G.P. Rodnan, Impairment of uric acid excretion in gout, J. Clin. Invest. 41 (1962) 1955.